Available online at www.sciencedirect.com
SCIENCE DIRECT®
Biochemical and Biophysical Research Communications 325 (2004) 250–256
BBRC
www.elsevier.com/locate/ybbrc

Endoplasmic reticulum stress and N-glycosylation modulate expression of WFS1 protein

Suguru Yamaguchi[a], Hisamitsu Ishihara[a,*], Akira Tamura[a], Takahiro Yamada[a], Rui Takahashi[a], Daisuke Takei[a], Hideki Katagiri[b], Yoshitomo Oka[a]

[a] *Division of Molecular Metabolism and Diabetes, Tohoku University Graduate School of Medicine, 2-1 Seiryo-machi, Aoba-ku, Sendai, Miyagi 980-8575, Japan*
[b] *Division of Advanced Therapeutics for Metabolic Diseases, Tohoku University Graduate School of Medicine, 2-1 Seiryo-machi, Aoba-ku, Sendai, Miyagi 980-8575, Japan*

Received 22 September 2004
Available online 22 October 2004

Abstract

Mutations of the *WFS1* gene are responsible for two hereditary diseases, Wolfram syndrome and low frequency sensorineural hearing loss. The WFS1 protein is a glycoprotein located in the endoplasmic reticulum (ER) membrane but its function is poorly understood. Herein we show WFS1 mRNA and protein levels in pancreatic islets to be increased with ER-stress inducers, thapsigargin and dithiothreitol. Another ER-stress inducer, the N-glycosylation inhibitor tunicamycin, also raised WFS1 mRNA but not protein levels. Site-directed mutagenesis showed both Asn-663 and Asn-748 to be N-glycosylated in mouse WFS1 protein. The glycosylation-defective WFS1 protein, in which Asn-663 and Asn-748 had been substituted with aspartate, exhibited an increased protein turnover rate. Consistent with this, the WFS1 protein was more rapidly degraded in the presence of tunicamycin. These data indicate that ER-stress and N-glycosylation play important roles in WFS1 expression and stability, and also suggest regulatory roles for this protein in ER-stress induced cell death.

Keywords: Wolfram syndrome; Low frequency sensorineural hearing loss; WFSI; ER-stress; N-Glycosylation

The *WFS1* gene, encoding a transmembrane protein of the endoplasmic reticulum (ER) [1], is mutated in two hereditary diseases, autosomal recessive Wolfram syndrome (OMIN:222300) [2,3] and autosomal dominant low frequency sensorineural hearing loss (LFSNHL) (OMIM:600965) [4,5]. The former is also known as DIDMOAD, summarizing the most frequent symptoms; diabetes insipidus, diabetes mellitus, optic atrophy, and deafness. More than 100 mutations of the *WFS1* gene have been identified to date in patients with these diseases [6]. WFS1 protein, also called wolframin, consists of 890 amino acids [2,3] and its homologues are found in several organisms; *Drosophila melanogaster* (CG4917), *Anopheles gambiae* (EBIP3764), *Ciona intestinalis* (Cin.16116), *Fugu rubripes* (SINFRUP82345), and *Xenopus laevis* (Xl.3995). However, these proteins share no homology with known proteins, making it difficult to speculate as to their functions.

We recently established a murine model with a disrupted *wfs1* gene [7]. Mutant mice exhibited impaired glucose homeostasis due to defective insulin secretion in vivo. Studies using isolated islets revealed that mutant islet cells were prone to apoptosis induced by insults which impair ER functions and trigger the so-called unfolded protein response (UPR) [8,9]. Therefore, it was suggested that WFS1 protein plays a role in modulation of apoptotic processes that arise from impairment of ER function [7]. In addition, isolated islets from WFS1-deficient mice exhibited defective insulin

* Corresponding author. Fax: +81 22 717 7612.
E-mail address: ishihara-tky@umin.ac.jp (H. Ishihara).

0006-291X/$ - see front matter © 2004 Elsevier Inc. All rights reserved.
doi:10.1016/j.bbrc.2004.10.017

secretion which was accompanied by decreased calcium responses to glucose. Conversely, wolframin-overexpressing islets showed increased insulin secretion, indicating that wolframin also participates in regulation of stimulus-secretion coupling in insulin exocytosis [7]. It has recently been reported that WFS1 protein/wolframin expression in *Xenopus* oocytes conferred cation channel activity and increased cytosolic calcium levels [10]. This observation is intriguing since intracellular calcium regulation plays important roles in modulating both apoptotic and exocytotic processes. Despite these advancements, however, little is known about the mechanisms by which WFS1 protein actually alters these processes.

To understand the role that WFS1 protein/wolframin plays in the regulation of apoptotic and exocytotic events as well as in other as yet unknown cellular processes, information on the structure and function of this protein must be obtained. The amino acid sequence suggests that WFS1 protein is a multi-membrane spanning protein with hydrophilic amino (N)- and carboxy (C)-terminal regions [2,3]. In addition, biochemical and immunocytochemical analyses showed WFS1 protein to be an ER membrane glycoprotein [1].

In the present studies, we first examined WFS1 protein expression after treatment with agents that trigger UPR. We found WFS1 mRNA and protein levels to be increased by thapsigargin or dithiothreitol (DTT). Treatment with tunicamycin, an inhibitor of N-glycosylation, also raised WFS1 mRNA levels, suggesting that UPR increases WFS1 mRNA levels. However, the WFS1 protein level is not increased by tunicamycin. Subsequent analyses demonstrated protein stability to be reduced in the glycosylation-defective WFS1 protein. These results contribute to further understanding of the functions of this enigmatic protein.

Materials and methods

Reagents and antibodies. Tunicamycin, thapsigargin, DTT, and anti-actin antibody were purchased from Sigma–Aldrich Japan (Tokyo, Japan). Anti-HA and anti-CHOP antibodies were obtained from Santa Cruz Biotechnology (Santa Cruz, CA). Anti-WFS1 N-terminus antibody was described previously [11].

Pancreatic islet isolation and treatment with ER-stress inducers. Pancreatic islets were isolated from male C57BL/6 mice by retrograde injection of collagenase (Sigma–Aldrich Japan, Tokyo, Japan) into the pancreatic duct. Approximately 100 (for Western blot analyses) or 200 (for RNA extraction) islets were treated with 2 μg/ml thapsigargin, 5 mM DTT, or 5 μM tunicamycin for 36 h in RPMI1640 medium. Total RNA was extracted using Isogen reagent (NipponGene, Toyama, Japan). Quantitative real-time PCR analysis for WFS1 mRNA levels was performed using primers, 5′-CTGGAAACTCAACCCCAAGA-3′ and 5′-TTGGATTCACTGCTGACGAG-3′.

Plasmids. pHA-mWFS1 encodes a fusion protein consisting of an initiator methionine, the HA epitope tag (YPYDVPDYA), and amino acids 2–890 of mouse WFS1 protein. To generate this plasmid, a fragment encoding a *Sal*I restriction site and amino acids 2–484 was amplified by PCR. Using the PCR method, pmWFS1-HA encoding mouse WFS1 protein with an HA tag between residues 830 and 831 was also generated. pHA-mWFS1(N633D) and pHA-mWFS1 (N748D), which encode HA-tagged WFS1 protein with a mutation of asparagine 633 to aspartate and asparagine 748 to aspartate, respectively, were generated using PCR-based mutagenesis on pHA-mWFS1. pHA-mWFS1(N633D/N748D) encoding a mutant protein with mutation of both asparagine residues was generated using pHA-mWFS1(N633D).

Cell culture and transient transfection. MIN6 [12] and COS7 cells were grown in Dulbecco's modified Eagle's medium (DMEM) supplemented with 10% (v/v) fetal calf serum, 50 U/ml penicillin, and 50 μg/ml streptomycin sulfate. Transfection of plasmids was carried out using FuGENE6 (Roche, Indianapolis, IN) diluted in OPTI media (Invitrogen, Carlsbad, CA). Cells were harvested for Western blot or proceeded to immunostaining analysis 36 h after transfection. Immunostaining was performed using anti-HA antibody and FITC-conjugated anti-mouse IgG (Jackson ImmunoResearch, West Grove, PA).

Trypsin treatment. COS7 cells transfected with either pHA-mWFS1 or pmWFS1-HA were homogenized in a buffer containing 270 mM sucrose, 2 mM EDTA, and 50 mM Hepes (pH 7.5). Cellular membranes were recovered by centrifuging the homogenate at 17,400*g* for 15 min. Membranes (100 μg) were then incubated with trypsin at various concentrations at 4 °C. After a 30 min incubation, homogenates were boiled and subjected to SDS/PAGE and Western blot analysis.

Endoglycosydase cleavage. COS7 cells transfected with either wild-type WFS1 cDNA or mutant constructs were dissolved in denaturing buffer (0.5% SDS, 1% β-mercaptoethanol), boiled for 10 min at 100 °C, then incubated at 37 °C for 1 h with endoglycosidase H (500 U), and subjected to electrophoresis on NuPAGE 3–8% Tris–acetate gel (Invitrogen).

Metabolic labeling. MIN6 cells were labeled with [^{35}S]methionine and [^{35}S]cysteine (100 μCi/ml; EXPRE^{35}S^{35}S labeling mix, Perkin–Elmer-New England Nuclear, Boston, MA) in DMEM with either methionine or cysteine in the presence or absence of 5 μg/ml tunicamycin for 3 h. Cells were then chased for different periods in complete medium with or without tunicamycin. COS7 cells transfected with pHA-mWFS1 or pHA-mWFS1(N633D/N748D) were also labeled with [^{35}S]methionine and [^{35}S]cysteine for 3 h. Cells were then chased for different periods in complete medium. MIN6 and COS7 cells were lysed in a buffer containing 100 mM NaCl, 0.5 mM EDTA, 20 mM Tris (pH 7.5), and 0.5% NP-40. Lysates were incubated with 10 μl protein A/G–Sepharose (Amersham Biosciences, Piscataway, NJ) for 2 h and then briefly centrifuged. The resulting supernatant was incubated with anti-WFS1 N-terminus or anti-HA antibodies overnight and then incubated with protein A/G–Sepharose for 2 h. The beads were washed three times and bound WFS1 proteins were eluted in SDS-sample buffer and subjected to SDS/PAGE (10%).

Statistical analyses. Data are presented as means ± SE. Differences were assessed by Student's *t* test.

Results and discussion

Effect of ER-stress inducers on WFS1 expression in pancreatic islets

We recently reported that WFS1-deficient islets exhibited increased susceptibility to apoptosis due to impaired ER function [7]. Therefore, in this study, we first determined WFS1 expression in isolated mouse pancreatic islets treated with the ER-stress inducers, thapsigargin, DTT, and tunicamycin. Thapsigargin is an inhibitor of the sarco(endo)plasmic reticulum Ca^{2+} pump and

depletes ER Ca^{2+}, which affects the functions of Ca^{2+}-dependent ER chaperone proteins. DTT and tunicamycin affect protein folding by disrupting disulfide bonds and inhibiting N-glycosylation, respectively. These compounds therefore cause mis-folding of proteins (ER-stress) and induce UPR [13]. As shown in Fig. 1, WFS1 protein expression was increased in islets treated with 2 μM thapsigargin (Fig. 1A) or 5 mM DTT (Fig. 1B) for 36 h. Greater than threefold increases in WFS1 mRNA levels were also observed by quantitative RT-PCR analyses in islets treated with these agents (data not shown). Another ER-stress inducer, tunicamycin (5 μg/ml), did not raise WFS1 protein levels in isolated islets (Fig. 1C). However, quantitative RT-PCR analyses revealed WFS1 mRNA levels to be increased by 72% in islets treated with tunicamycin (Fig. 1D). These data suggest that WFS1 mRNA expression increases in response to the ER-stress.

WFS1 protein has been shown to be a glycoprotein [1] like the inositol trisphosphate receptor, another ER membrane resident protein essential for cellular calcium homeostasis and signaling [14]. The unaltered WFS1 protein levels despite increased mRNA levels in islets treated with tunicamycin raise the possibility that inhibition of N-glycosylation affects WFS1 protein stability. To address this possibility, pancreatic β-cell derived MIN6 cells were labeled for 3 h with [^{35}S]methionine/cysteine and chased with unlabeled methionine and cysteine for different intervals in the continuous absence or presence of tunicamycin. As shown in Fig. 1E, WFS1 protein in tunicamycin-treated cells was more rapidly degraded, suggesting that inhibition of N-glycosylation reduces WFS1 protein stability.

Membrane topology of WFS1 protein

To study the roles of N-glycosylation more specifically, we first sought to determine N-glycosylation site(s) of WFS1 protein/wolframin. Since N-glycosylation occurs in the ER, it was prerequisite to know the membrane topology of this protein. The initial hydropathy plot studies did not provide a definitive answer; WFS1 protein contains 9 or 10 transmembrane segments, with long hydrophilic stretches on both the N- and the C-termini [2,3].

To localize the N- and the C-termini of WFS1 protein with respect to the ER membrane, we transiently expressed, in COS7 cells, mouse WFS1 protein tagged with an HA-epitope in either the N- or the C-terminal stretch (designated HA-mWFS1 or mWFS1-HA, respectively,

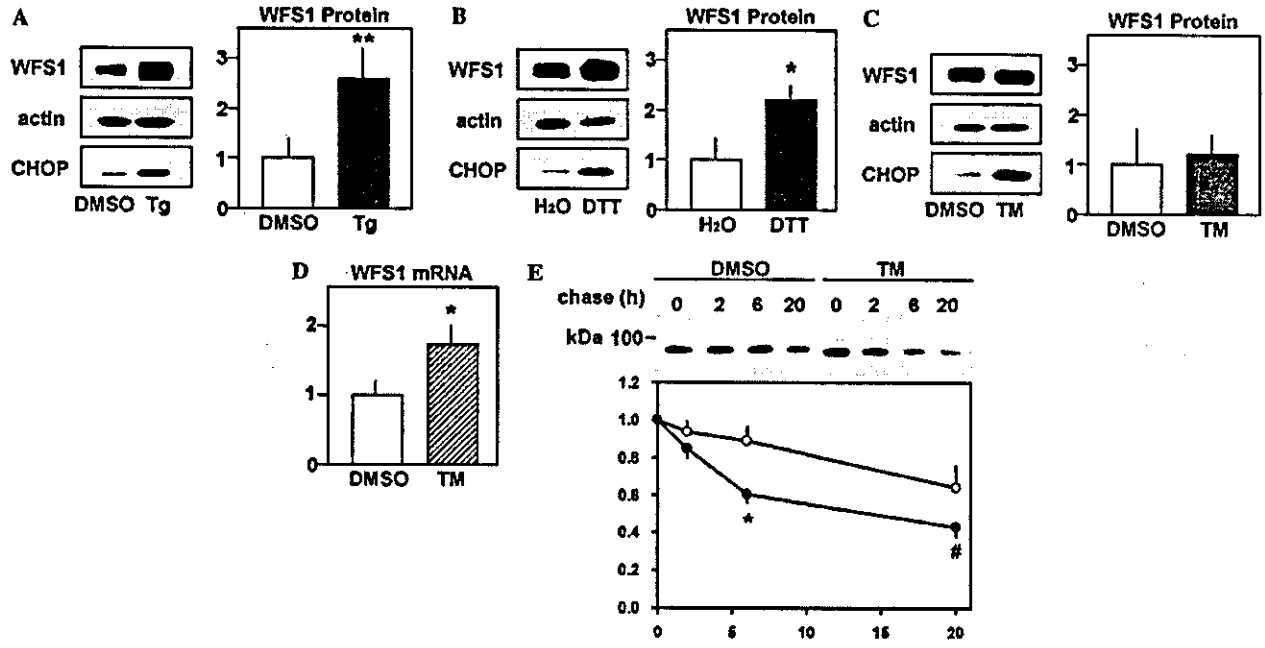

Fig. 1. WFS1 expression in mouse pancreatic islets in response to ER-stress inducers. (A–C) Isolated mouse islets were challenged with 2 μM thapsigargin (Tg) (A, $n = 4$), 5 mM DTT (B, $n = 3$) or 5 μg/ml tunicamycin (TM) (C, $n = 5$). After a 36-h incubation, the islets were subjected to SDS/PAGE and blotted using antibodies against the WFS1 N-terminus, actin, or CHOP. Representative blots are shown in the left panels. Increased CHOP expression indicated successful induction of ER-stress mediated apoptosis. WFS1 protein/actin levels are summarized in the right panels. Data are expressed as the expression relative to those of a control islet preparation. (D) Total RNA was extracted from isolated mouse islets treated with 5 μg/ml tunicamycin for 36 h. WFS1 and GAPDH mRNA levels were determined by quantitative real-time PCR. WFS1 mRNA levels were normalized to those of GAPDH. Data were obtained using three independent sets of islet preparations. (E) MIN6 cells were pulse-labeled for 3 h without or with 5 μg/ml tunicamycin and chased for up to 20 h in the continuous absence or presence of the drug. A representative result from three independent experiments is shown in the upper panel. Data from three experiments are summarized, after normalization to time zero of the chase in the lower panel. Open circles, DMSO-treated MIN6 cells. Closed circles, tunicamycin-treated cells. $^{\#}P = 0.0634$, $^{*}P < 0.05$, $^{**}P < 0.01$.

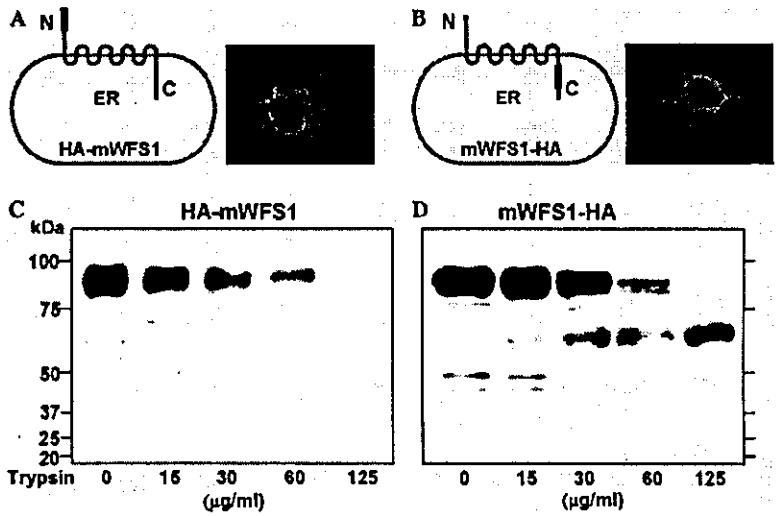

Fig. 2. Membrane orientations of the N- and the C-termini of WFS1 protein as determined by trypsin proteolysis. WFS1 protein tagged with the HA epitope at either the N- (A,C) or the C-terminus (B,D) was expressed in COS7 cells. (A,B) Schematic illustration and immunocytochemical demonstration of the HA-tagged WFS1 proteins used in (C) and (D). (C,D) Membranes from COS7 cells transfected with a plasmid encoding either HA-mWFS1 or mWFS1-HA were treated with the indicated amounts of trypsin. After incubation for 30 min at 4 °C, the reactions were stopped by boiling for 5 min, and subjected to SDS/PAGE and immunoblot analysis with anti-HA antibody.

Figs. 2A and B). HA-mWFS1 and mWFS1-HA proteins were successfully expressed and localized to the ER, as demonstrated by reticular staining in the cytoplasm (Figs. 2A and B). Membrane preparation of cells expressed with either HA-mWFS1 or mWFS1-HA proteins was then subjected to trypsin digestion followed by SDS/PAGE and immunoblotting with an antibody against the HA epitope. The HA-epitope tagged at the N-terminus was completely digested with increasing concentrations of trypsin (Fig. 2C). This was not due to loss of membrane vesicle integrity, since no changes in an ER-resident chaperone protein, GRP78, were detected using an antibody against GRP78 in the same membrane preparations (data not shown). In contrast, the C-terminal HA epitope was protected from trypsin (Fig. 2D). These results indicated that WFS1 protein has odd numbers of transmembrane segments with the orientation of the N-terminus toward the cytoplasm and that of the C-terminus toward the ER lumen. A similar conclusion was obtained by trypsin-digestion of the membrane, followed by detection with C-terminal or N-terminal antibodies [15].

Determination of N-glycosylation sites.

Mouse WFS1 protein has six asparagine residues with the consensus sequence for N-glycosylation (N-X-S/T, where X is any amino acid except for proline). According to a 9-transmembrane model with N-terminus cytosolic/C-terminus luminal orientation, asparagines 663 and 748 would be localized in the ER. Therefore, we mutated these two asparagine residues to aspartate in order to determine whether one or both are N-linked glycosylation site(s). Mutant WFS1 proteins in which asparagine 663 and/or asparagine 748 was mutated to aspartate [designated HA-mWFS1(N663D), HA-mWFS1(N748D), and HA-mWFS1(N663D/N748D)] were successfully expressed in the ER (Fig. 3A). When these WFS1 mutant proteins were subjected to SDS/PAGE, HA-mWFS1(N663D/N748D) migrated faster than the HA-wild-type mWFS1 protein, while both HA-mWFS1(N663D) and HA-mWFS1(N748D) mutants were between the two (Fig. 3B). These results suggested that both asparagine residues, 663 and 748, are glycosylation sites and place the C-terminal stretch of WFS1 protein within the intraluminal compartment. Furthermore, as shown in Fig. 3C, although endoglycosidase H (Endo H) treatment of the wild-type WFS1 protein resulted in faster migration of the protein, the mobility of the double mutant [WFS1 (N663D/N748D)] protein was not affected by treatment with Endo H. In addition, the double mutant protein exhibited the same mobility as the wild-type WFS1 protein treated with Endo H. These data demonstrated that no asparagine residue other than N663 and N748 is glycosylated.

Reduced protein stability of N-glycosylation-defective WFS1 protein

N-glycosylation reportedly plays an important role in the stability of proteins such as the T cell antigen receptor α-subunit [16], the α-subunit of the nicotinic acetylcholine receptor [17], and apolipoprotein B [18]. Therefore, to assess the role of N-glycosylation in WFS1 protein stability, we performed pulse-chase

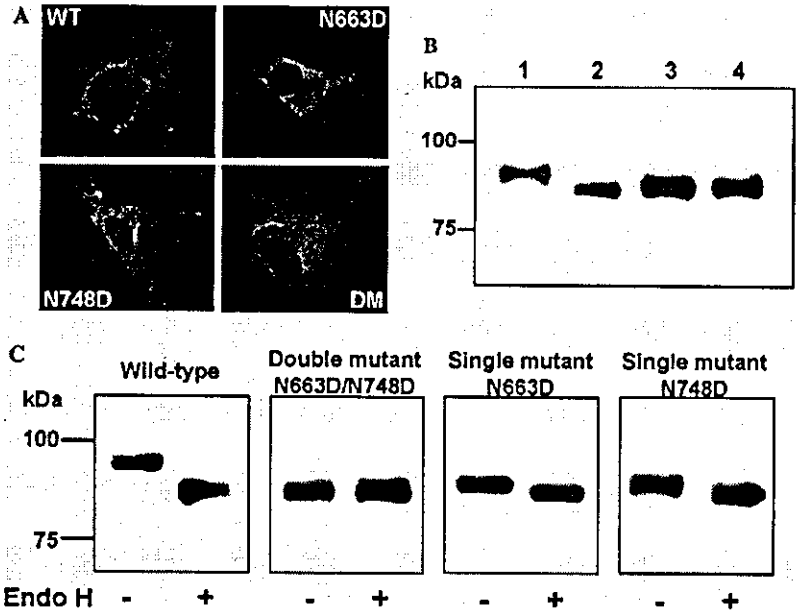

Fig. 3. Electrophoretic mobility and effect of endoglycosidase digestion on HA-tagged wild-type and mutant WFS1 proteins. (A) Immunofluorescence localization of HA-tagged WFS1 proteins: upper left, wild-type HA-mWFS1; upper right, HA-mWFS1(N663D); lower left, HA-mWFS1(N748D); lower right, HA-mWFS1(N663D/N748D). (B) COS7 cells transfected with 0.5 μg plasmids encoding either HA-tagged wild-type or mutant WFS1 proteins were lysed, subjected to SDS/PAGE, and probed with anti-HA antibody: lane 1, HA-mWFS1; lane 2, HA-mWFS1 (N663D/N748D); lane 3, HA-mWFS1(N663D); and lane 4, HA-mWFS1(N748D). (C) Lysates of COS7 cells transfected with either wild-type WFS1 cDNA or mutant constructs were incubated at 37 °C for 1 h with or without endoglycosidase H (500 U) and were subjected to electrophoresis on NuPAGE 3–8% Tris–acetate gel.

experiments. In these experiments, COS7 cells transiently transfected with either the HA-wild-type mWFS1 or mutant HA-mWFS1(N663D/N748D) cDNAs were labeled for 3 h with [^{35}S]methionine/cysteine and chased for different intervals. As shown in Fig. 4, the wild-type mWFS1 protein was relatively stable; 65 ± 6% ($n = 3$) of the protein remained 18 h after its synthesis. In contrast, only 44 ± 5% ($n = 3$) of mWFS1(N663D/N748D) remained after 18 h. These data showed protein stability to be reduced when both N-glycosylation sites were disrupted. One could argue an increased turnover rate of mWFS1(N663D/N748D) to be due to introducing aspartate residues rather than lack of glycosylation. To study the roles of N-glycosylation in various glycoproteins, asparagine residues in the consensus motif have been substituted with a variety of amino acids, such as aspartate ([19,20], this study), glutamine [14,21], alanine [19,22], threonine [23], and isoleucine [24]. None of these replacements were perfect, because introducing different residues might have its own effects. In this study, we also observed that WFS1 protein in MIN6 cells was more rapidly degraded when treated with a glycosylation inhibitor, tunicamycin (Fig. 1E). Thus, both molecular and biochemical approaches indicated that glycosylation-defective WFS1 protein has reduced stability. We therefore conclude that N-glycosylation affects WFS1 protein levels. A previous study using the ER resident glycoprotein ribophorin showed N-glycosylation to be necessary for calnexin binding, which prevents the glycoprotein from being rapidly degraded [25]. Such a mechanism could also be operative in WFS1 protein.

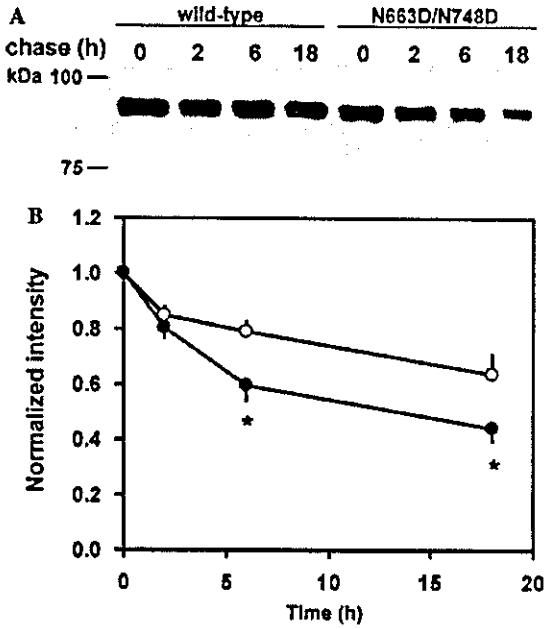

Fig. 4. Decreased stability of glycosylation-defective WFS1 protein. (A) HA-mWFS1 and HA-mWFS1(N663D/N748D) profiles of radiolabeled bands as a function of time of chase. A representative result from three experiments is shown. (B) Data from three experiments are summarized after normalization to time zero of chase. *$P < 0.05$.

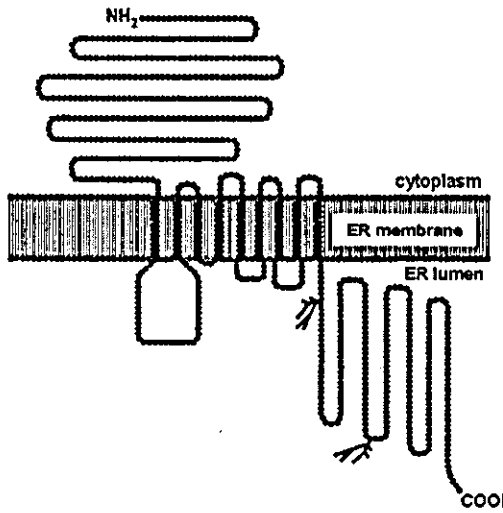

Fig. 5. Transmembrane topology model for mouse WFS1 protein with glycosylation sites. Membrane topology of mouse WFS1 protein as based on analysis using the SOSUI computer program [26] and data obtained in this study. Two N-glycosylation sites in the C-terminus stretch are depicted.

Herein, we defined the membrane topology of WFS1 by analyzing protease protection susceptibility: the orientation of the N-terminus in the cytoplasm and the C-terminus in the ER. This topology was supported by determining the N-glycosylation sites to be N663 and N748. A schematic diagram of WFS1 protein deduced from the current study and others is shown in Fig. 5. WFS1 protein/wolframin is a type II transmembrane protein and has long N-terminal and C-terminal stretches. These stretches could interact with other molecule(s), thereby mediating specific functions. Further study of these actions is clearly warranted. N663 and N748 residues in murine WFS1 protein correspond to N661 and N746 in the human orthologue. Although more than 100 mutations have been identified in WFS1 protein/wolframin and span the entire coding sequence, no mutations in these asparagine residues or adjacent amino acids were found in patients with Wolfram syndrome or LFSNHL. Given that loss of the functions of this protein is at least one of the pathogenic mechanisms of Wolfram syndrome [6,15], future survey of genomic sequences in patients with these diseases might identify mutations in these glycosylation sites.

The present data also provide evidence that increased WFS1 expression is the primary response of this protein to ER stress. There is no increase in WFS1 protein expression in response to tunicamycin, despite increased WFS1 mRNA levels. This is apparently attributable to the combined effects of increased mRNA levels and reduced protein stability. The increased WFS1 expression in response to ER-stress raises the possibility that WFS1 protein is a component of the UPR and plays a protective role against ER stress. This notion is supported by our recent findings that islets isolated from WFS1-deficient mice exhibited increased susceptibility to ER stress-induced apoptosis [7].

Acknowledgments

We are grateful to Y. Nagura for her expert technical assistance. This work was supported by a grant from Suzuken Memorial Foundation to H.I. and a Grant-in-Aid for Scientific Research (13204062) to Y.O. from the Ministry of Education, Science, Sports and Culture of Japan.

References

[1] K. Takeda, H. Inoue, Y. Tanizawa, Y. Matsuzaki, J. Oba, Y. Watanabe, K. Shinoda, Y. Oka, WFS1 (Wolfram syndrome 1) gene product: predominant subcellular localization to endoplasmic reticulum in cultured cells and neuronal expression in rat brain, Hum. Mol. Genet. 10 (2001) 477–484.

[2] H. Inoue, Y. Tanizawa, J. Wasson, P. Behn, K. Kalidas, E. Bernal-Mizrachi, M. Mueckler, H. Marshall, H. Donis-Keller, P. Crock, D. Rogers, M. Mikuni, H. Kimashiro, K. Higashi, G. Sobue, Y. Oka, M.A. Permutt, A gene encoding a transmembrane protein is mutated in patients with diabetes mellitus and optic atrophy (Wolfram syndrome), Nat. Genet. 20 (1998) 143–148.

[3] T.M. Strom, K. Hoetnagael, S. Hofmann, F. Gekeler, C. Scharfe, W. Rabl, K.D. Gerbitz, T. Meitinger, Diabetes insipidus, diabetes mellitus, optic atrophy and deafness (DIDMOAD) caused by mutations in a novel gene (wolframin) coding for a predicted transmembrane protein, Hum. Mol. Genet. 7 (1998) 2021–2028.

[4] I.N. Bespalova, G. Van Camp, S.J. Bom, D.J. Brown, K. Cryns, A.T. DeWan, A.E. Erson, K. Flothmann, H.P. Kunst, P. Kurnool, T.A. Sivakumaran, W.W.R.J. Cremers, S.M. Leal, M. Burmeister, M.M. Lesperance, Mutations in the Wolfram syndrome 1 gene (*WFS1*) are a common cause of low frequency sensorineural hearing loss, Hum. Mol. Genet. 15 (2001) 2501–2508.

[5] T.L. Young, E. Ives, E. Lynch, R. Person, S. Snook, L. MacLaren, T. Cater, A. Griffin, B. Fernandez, M.K. Lee, M.-C. King, Non-syndromic progressive hearing loss DFNA38 is caused by heterozygous missense mutation in the Wolfram syndrome gene WFS1, Hum. Mol. Genet. 15 (2001) 2509–2514.

[6] K. Cryns, T.A. Sivakumaran, J.M. Van den Ouweland, R.J. Pennings, C.W. Cremers, K. Flothmann, T.L. Young, R.J. Smith, M.M. Lesperance, G. Van Camp, Mutational spectrum of the WFS1 gene in Wolfram syndrome, nonsyndromic hearing impairment, diabetes mellitus, and psychiatric disease, Hum. Mutat. 22 (2003) 275–287.

[7] H. Ishihara, S. Takeda, A. Tamura, R. Takahashi, S. Yamaguchi, D. Takei, T. Yamada, H. Inoue, H. Soga, H. Katagiri, Y. Tanizawa, Y. Oka, Disruption of the WFS1 gene in mice causes progressive beta-cell loss and impaired stimulus-secretion coupling in insulin secretion, Hum. Mol. Genet. 13 (2004) 1159–1170.

[8] R. Kaufmann, Orchestrating the unfolded protein response in health and disease, J. Clin. Invest. 110 (2002) 1389–1398.

[9] H.P. Harding, D. Ron, Endoplasmic reticulum stress and the development of diabetes, Diabetes 51 (Suppl. 3) (2002) S455–S461.

[10] A.A. Osman, M. Saito, C. Makepeace, M.A. Permutt, P. Schlesinger, M. Mueckler, Wolframin expression induces novel ion channel activity in endoplasmic reticulum membranes and increases intracellular calcium, J. Biol. Chem. 278 (2003) 52755–52762.

[11] K. Cryns, S. Thys, L. van Laer, Y. Oka, M. Pfister, L. van Nassauw, R.J.H. Smith, J.P. Timmermans, G. Van Camp, The WFS1 gene, responsible for low frequent sensorineural hearing loss and Wolfram syndrome, is expressed in a variety of inner ear cells, Histochem. Cell Biol. 119 (2003) 247–256.
[12] H. Ishihara, T. Asano, K. Tsukuda, H. Katagiri, K. Inukai, M. Anai, M. Kikuchi, Y. Yazaki, J.I. Miyazaki, Y. Oka, Pancreatic beta cell line MIN6 exhibits characteristics of glucose metabolism and glucose-stimulated insulin secretion similar to those of normal islets, Diabetologia 36 (1993) 1139–1145.
[13] K.F. Ferri, G. Koemer, Organelle-specific initiation of cell death pathways, Nat. Cell Biol. 3 (2001) E255–E263.
[14] T. Michikawa, H. Hamanaka, H. Otsu, A. Yamamoto, A. Miyawaki, T. Furuichi, Y. Tashiro, K. Mikoshiba, Transmembrane topology and sites of N-glycosylation of inositol 1,4,5-trisphosphate receptor, J. Biol. Chem. 269 (1994) 9184–9189.
[15] S. Hofmann, C. Philbrook, K.D. Gerbitz, M.F. Bauer, Wolfram syndrome: structural and functional analyses of mutant and wild-type wolframin, the WFS1 gene product, Hum. Mol. Genet. 12 (2003) 2003–2012.
[16] K.P. Kearse, D.B. Williams, A. Singer, Persistence of glucose residues on core oligosaccharides prevents association of TCR alpha and TCR beta proteins with calnexin and results specifically in accelerated degradation of nascent TCR alpha proteins within the endoplasmic reticulum, EMBO J. 273 (1994) 17064–17072.
[17] S.H. Keller, J. Lindstrom, P. Taylor, Inhibition of glucose trimming with castanospermine reduces calnexin association and proteosome degradation of the alpha-subunit of the nicotinic acetylcholine receptor, J. Biol. Chem. 273 (1998) 17064–17072.
[18] Y. Chen, F. Caherec, S.L. Chuck, Calnexin and other factors that alter translocation affects the rapid binding of ubiquitin to apoB in the Sec61 complex, J. Biol. Chem. 273 (1998) 11887–11894.
[19] T.K. Lee, A.S. Koh, Z. Cui, R.H. Pierce, N. Ballatori, N-glycosylation controls functional activity of Oatp1, an organic anion transporter, Am. J. Physiol. Gastrointest. Liver Physiol. 285 (2003) G371–G381.
[20] L. Niu, M.L. Heancy, J.C. Vera, D.W. Golde, High-affinity binding to the GM-CSF receptor requires intact N-glycosylation sites in the extracellular domain of the β subunit, Blood 95 (2000) 3357–3362.
[21] Q. Gong, C.L. Anderson, C.T. January, Z. Zhou, Role of glycosylation in cell surface expression and stability of HERG potassium channels, Am. J. Physiol. Heart Circ. Physiol. 283 (2002) H77–H84.
[22] J. He, A.M. Castleberry, A.G. Lau, R.A. Hall, Glycosylation of β_1-adrenergic receptors regulates receptor surface expression and dimerization, Biochem. Biophys. Res. Commun. 297 (2002) 565–572.
[23] N. Buhlmamm, A. Aldecoa, K. Leuthauser, R. Gujer, R. Muff, J.A. Fischer, W. Born, Glycosylation of the calcitonin receptor-like receptor at Asn(60) or Asn(112) is important for cell surface expression, FEBS Lett. 486 (2000) 320–324.
[24] M. Ramanujam, J. Hofmann, H.L. Nakhasi, C.D. Atreya, Effect of site-directed asparagine to isoleucine substitutions at the N-linked E1 glycosylation sites on rubella virus viability, Virus Res. 81 (2001) 151–156.
[25] M. de Virgilio, C. Kitzmueller, E. Schwaiger, M. Klein, G. Kreibich, N.E. Ivessa, Degradation of a short-lived glycoprotein from the lumen of the endoplasmic reticulum: the role of N-inked glycans and the unfolded protein response, Mol. Biol. Cell 10 (1999) 4059–4073.
[26] T. Hirokawa, S. Boon-Chieng, S. Mitaku, SOSUI: classification and secondary structure prediction system for membrane proteins, Bioinformatics 14 (1998) 378–379.

Perspectives in Diabetes

Dissipating Excess Energy Stored in the Liver Is a Potential Treatment Strategy for Diabetes Associated With Obesity

Yasushi Ishigaki,[1] Hideki Katagiri,[2] Tetsuya Yamada,[1] Takehide Ogihara,[2] Junta Imai,[1,2] Kenji Uno,[1,2] Yutaka Hasegawa,[1,2] Junhong Gao,[1,2] Hisamitsu Ishihara,[1] Tooru Shimosegawa,[3] Hideyuki Sakoda,[4] Tomoichiro Asano,[4] and Yoshitomo Oka[1]

For examining whether dissipating excess energy in the liver is a possible therapeutic approach to high-fat diet–induced metabolic disorders, uncoupling protein-1 (UCP1) was expressed in murine liver using adenoviral vectors in mice with high-fat diet–induced diabetes and obesity, and in standard diet–fed lean mice. Once diabetes with obesity developed, hepatic UCP1 expression increased energy expenditure, decreased body weight, and reduced fat in the liver and adipose tissues, resulting in markedly improved insulin resistance and, thus, diabetes and dyslipidemia. Decreased expressions of enzymes for lipid synthesis and glucose production and activation of AMP-activated kinase in the liver seem to contribute to these improvements. Hepatic UCP1 expression also reversed high-fat diet–induced hyperphagia and hypothalamic leptin resistance, as well as insulin resistance in muscle. In contrast, intriguingly, in standard diet–fed lean mice, hepatic UCP1 expression did not significantly affect energy expenditure or hepatic ATP contents. Furthermore, no alterations in blood glucose levels, body weight, or adiposity were observed. These findings suggest that ectopic UCP1 in the liver dissipates surplus energy without affecting required energy and exerts minimal metabolic effects in lean mice. Thus, enhanced UCP expression in the liver is a new potential therapeutic target for the metabolic syndrome. ***Diabetes*** **54:322–332, 2005**

From the [1]Division of Molecular Metabolism and Diabetes, Tohoku University Graduate School of Medicine, Sendai, Japan; the [2]Division of Advanced Therapeutics for Metabolic Diseases, Center for Translational and Advanced Animal Research, Tohoku University Graduate School of Medicine, Sendai, Japan; the [3]Division of Gastroenterology, Tohoku University Graduate School of Medicine, Sendai, Japan; and the [4]Department of Internal Medicine, Faculty of Medicine, University of Tokyo, Tokyo, Japan.

Address correspondence and reprint requests to Hideki Katagiri, MD, PhD, Division of Advanced Therapeutics for Metabolic Diseases, Center for Translational and Advanced Animal Research, Tohoku University Graduate School of Medicine, 2-1 Seiryo-machi, Aoba-ku, Sendai 980-8575, Japan. E-mail: katagiri-tky@umin.ac.jp.

Received for publication 19 April 2004 and accepted in revised form 13 October 2004.

Y.I., H.K., and T.Y. contributed equally to this work.

ACC1, acetyl-CoA carboxylase 1; AMPK, AMP-activated protein kinase; CPT1, carnitine palmitoyltransferase 1; IRS1, insulin receptor substrate 1; PPAR, peroxisome proliferator–activated receptor; SREBP, sterol regulatory element binding protein; TNF-α, tumor necrosis factor-α; UCP, uncoupling protein.

An explosive increase in the number of diabetic patients, which has become a major public health concern in most industrialized countries in recent decades (1), is mainly the result of excess energy intake and physical inactivity. When food intake chronically exceeds metabolic needs, efficient metabolism causes excess energy storage and results in obesity, a common condition associated with diabetes, hyperlipidemia, and premature heart disease. Excess energy in cells lowers the response to insulin, namely insulin resistance. However, the major treatment modalities for diabetes, including insulin injection and oral sulfonylureas, aim at lowering blood glucose levels by driving glucose into cells in peripheral tissues such as muscle and fat. This further exacerbates insulin resistance when energy intake is in excess, resulting in a vicious cycle. Therefore, novel therapies that promote increased energy expenditure are needed.

Inefficient metabolism, such as the generation of heat instead of ATP, is a potential treatment strategy for type 2 diabetes associated with obesity. Uncoupling proteins (UCPs) were discovered members of the mitochondrial inner membrane carrier family. These proteins leak protons into the mitochondrial matrix, dissipating energy as heat rather than allowing it to be captured in ATP (2). UCP1 (thermogenin) was originally identified in brown adipose tissue and demonstrated to mediate nonshivering thermogenesis. UCP1 plays an important role in mediating cold exposure–induced thermogenesis (3) and is also a likely regulator of diet-induced thermogenesis (4).

Several laboratories have reported overexpression of UCPs, using the transgenic approach, in mice (5–8). These reports indicate that overexpression of UCPs in white adipose tissue and skeletal muscle has preventive effects on development of genetic and dietary obesity and the resultant insulin resistance. However, it is still unclear whether ectopic UCP1 expression exerts therapeutic effects after the development of diabetes associated with obesity.

The liver is one of the major metabolic organs involved in glucose and lipid metabolism and insulin action. In addition, the liver can store and release abundant fat

TABLE 1
Sequences of quantitative RT-PCR primers

Probe	Primer 1	Primer 2
FAS	5'-tgctcccagctgcaggc-3'	5'-gcccggtagctctgggtgta-3'
SCD-1	5'-tgggttggctgcttgtg-3'	5'-gcgtgggcaggatgaag-3'
SREBP1c	5'-catggattgcacatttgaag-3'	5'-cctgtgtcccctgtctca-3'
FAT	5'-tggctaaatgagactgggacc-3'	5'- acatcaccactccaatcccaag-3'
MCAD	5'-tcgaaagcggctcacaagcag-3'	5'-caccgcagctttccggaatgt-3'
UCP2	5'-cattctgaccatggtgcgtactga-3'	5'-gttcatgtatctcgtcttgaccac-3'
PPAR-α	5'-ggatgtcacacaatgcaattcgc-3'	5'-tcacagaacggcttcctcaggt-3'
PEPCK	5'-agcggatatggtgggaac-3'	5'-ggtctccactccttgttc-3'
G6Pase	5'-aaagagactgtgggcatcaatc-3'	5'-aatgcctgacaagactccagcc-3'
GAPDH	5'-accacagtccatgccatcac-3'	5'-tccaccaccctgttgctgta-3'

FAS, fatty acid synthase; SCD1, stearoyl-CoA desaturase 1; FAT, fatty acid transporter; MCAD, medium-chain acyl-CoA dehydrogenase; PEPCK, phosphoenolpyruvate carboxylase; G6Pase, glucose-6-phosphatase; GAPDH, glyceraldehyde-3-dehydrogenase.

dynamically, in response to the energy balance. We reported that hepatic AKT activation resulted in marked alterations in glucose and lipid metabolism (9), suggesting that the liver is a potential site of ectopic expression. We herein expressed UCP1 protein in the liver, before or after diabetes associated with dietary obesity had developed. We found that hepatic UCP1 expression improved diabetes and obesity under high-fat diet conditions through local effects in the liver as well as remote effects in adipose tissues, muscle, and the hypothalamus. However, in standard diet–fed lean mice, effects on glucose and lipid metabolism were minimal. Using gene transduction after disease development, as in this study, provides useful information allowing analysis of therapeutic, rather than preventive, effects that would be difficult to examine using congenitally gene-engineered animal models.

RESEARCH DESIGN AND METHODS

Preparation of recombinant adenovirus. Murine UCP1 cDNA (10) was provided by Professor Leslie P. Kozak (Pennington Biomedical Research Center). Murine liver carnitine palmitoyltransferase 1 (CPT1a) cDNA was obtained by RT-PCR with liver total RNA and primers designed from the reported sequence (GenBank accession no. NM_013495). Recombinant adenovirus, containing murine UCP1 (11) or CPT1a cDNA under the CAG promoter, was prepared as described previously (12). A recombinant adenovirus bearing the bacterial β-galactosidase gene (*AdexlCAlacZ*) (13) was used as a control.

Animals. Animal studies were conducted under protocols in accordance with the institutional guidelines for animal experiments at Tohoku University. Male C57BL/6N mice were housed individually and divided into high-fat diet (32% safflower oil, 33.1% casein, 17.6% sucrose, and 5.6% cellulose [14]) and standard diet (65% carbohydrate, 4% fat, and 24% protein) groups at 5 weeks of age, when body weights were 21.2 ± 0.25 g (means ± SE). Four weeks after separation, body weight–matched mice for each group received an injection of adenovirus via the tail vein. Viruses were administered intravenously at a dose of 2×10^8 plaque-forming units. For pair-feeding experiments, after 4 weeks of high-fat diet, mice were allotted into three groups. Two groups of mice received an injection of UCP1 or LacZ adenovirus. After 24 h, mice in the third group received an injection of LacZ adenovirus. The latter LacZ mice were given their daily food allotments on the basis of the previous day's consumption by UCP1 mice.

Antibodies. UCP1, acetyl-CoA carboxylase 1 (ACC 1), and insulin receptor antibodies were purchased from Santa Cruz Biotechnology (Santa Cruz, CA). The α-subunit of AMP-activated protein kinase (AMPK), phospho-AMPK (Thr172), and phospho-ACC (Ser79) antibodies were purchased from Cell Signaling Technology (Beverly, MA). Affinity-purified antibody against insulin receptor substrate 1 (IRS1) was prepared as described previously (15).

Immunoblotting. Tissue samples were prepared as previously described (9), and tissue protein extracts (250 μg of total protein) were boiled in Laemmli buffer that contained 10 mmol/l dithiothreitol and subjected to SDS-PAGE. The immunoblots were visualized with an enhanced chemiluminescence detection kit (Amersham, Buckinghamshire, U.K.).

Triglyceride content of the liver. Frozen livers were homogenized, and triglycerides were extracted with $CHCl_3$:CH_3OH (2:1, vol:vol), dried, and resuspended in 2-propanol (16). Triglyceride contents were measured using Lipidos liquid (TOYOBO, Osaka, Japan).

Oxygen consumption. Oxygen consumption was measured with an O_2/CO_2 metabolism measuring system (model MK-5000RQ; Muromachikikai, Tokyo, Japan). Each mouse was kept unrestrained in a sealed chamber with an air flow of 0.5 l/min for 5 h at 25°C without food or water during the light cycle. Air was sampled every 3 min, and the consumed oxygen concentration (Vo_2) was calculated.

Histological analysis. Livers as well as epididymal fat (white adipose tissue) and brown adipose tissues were removed and fixed with 10% formalin and embedded in paraffin. Tissue sections were stained with hematoxylin and eosin. Total adipocyte areas were traced manually and analyzed. Brown and white adipocyte areas were measured in 100 or more cells per mouse in each group.

Measurement of body temperature. Rectal temperature was measured with a Thermalert TH-5 (Physitemp, Clifton, NJ).

Measurement of ATP. The ATP levels in liver homogenates were measured with a luciferase-luciferin system (17) by using an ATP determination kit (Molecular Probes, Eugene, OR).

Measurement of AMPK activity. Livers were homogenized, and aliquots of supernatant were incubated with anti-AMPK α-subunit antibody. AMPK activity in the immunoprecipitates was assessed as a function of SAMS peptide phosphorylation, as previously described (18).

Tyrosine phosphorylation of insulin receptor and IRS1. Mice that were fasted for 16 h received an injection of 100 μl of normal saline (0.9% NaCl), with or without 10 units/kg body wt insulin, via the tail vein. Hindlimb muscles were removed 300 s later and immediately homogenated. After centrifugation, the resultant supernatants were used for immunoprecipitation with anti–insulin receptor or anti-IRS1 antibody. Immunoprecipitates were subjected to SDS-PAGE and then immunoblotted using anti-phosphotyrosine antibody (4G10) or individual antibodies as described previously (15).

Blood analysis. Blood glucose was assayed with Antsense II (Horiba Industry, Kyoto, Japan). Serum insulin and leptin were determined with ELISA kits (Morinaga Institute of Biological Science, Yokohama, Japan). Serum adiponectin and tumor necrosis factor-α (TNF-α) concentrations were measured with an ELISA kit (Ohtsuka Pharmaceutical, Tokyo, Japan) and a TNF-α assay kit (Amersham Biosciences, Uppsala, Sweden), respectively. Serum total cholesterol, triglyceride, and free fatty acid concentrations were determined with a Cholescolor liquid, Lipidos liquid (TOYOBO), and NEFA C (Wako Pure Chemical, Osaka, Japan) kits, respectively.

Glucose, insulin, and leptin tolerance tests. Glucose tolerance tests were performed on fasted (10 h) mice. Mice were given oral glucose (2 g/kg body wt), and blood glucose was assayed immediately before and at 15, 30, 60, and 120 min after administration. Insulin tolerance tests were performed on fed mice. Mice received an injection of human regular insulin (0.75 units/kg body wt; Eli Lilly, Kobe, Japan) into the intraperitoneal space, and blood glucose was assayed immediately before and at 20, 40, 60, and 80 min after injection. Leptin tolerance tests were performed as reported previously (19) with slight modification. Fasted (12 h) mice received an injection of mouse leptin (7.2 mg/kg body wt; R&D Systems) into the intraperitoneal space, and food intake amounts for 12 h thereafter were determined. Ratios of food intake amounts to those of vehicle-injected mice were calculated.

Quantitative RT-PCR–based gene expression. Total RNA was isolated from 0.1 g of mouse hepatic tissue with ISOGEN (Wako Pure Chemical), and

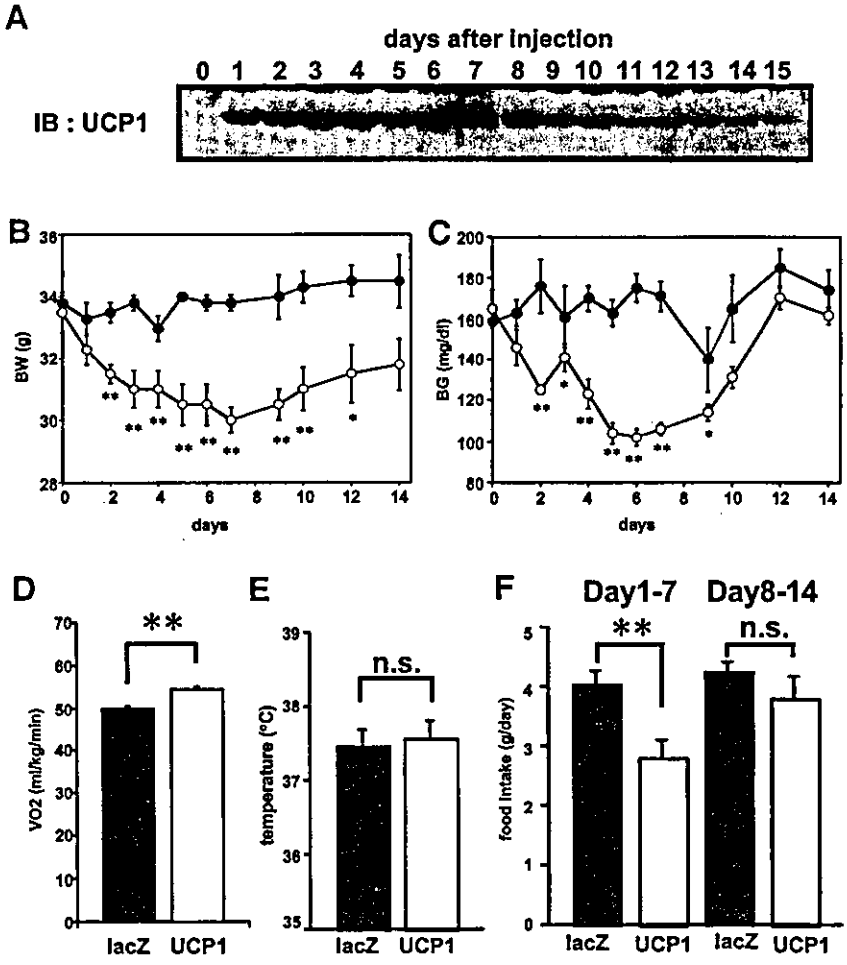

FIG. 1. Hepatic UCP1 expression reduced body weight and blood glucose levels. *A*: Ectopic UCP1 expression in the liver in high-fat–fed mice was detected by immunoblotting of hepatic extracts (250 μg total protein/lane). Liver samples were collected at different times after adenovirus injection. *B* and *C*: Body weights (*B*) and blood glucose levels (*C*) in the ad libitum–fed state after adenoviral administration in control (LacZ) mice (●) and UCP1 mice (○; n = 4 per group). *D*: Resting Vo_2 was measured on day 3 after adenoviral injection with open-circuit indirect calorimetry. All mice were kept in a cage for ~5 h in the daytime without food or water (n = 5 per group). *E*: Rectal temperature was measured in the ad libitum–fed state on day 7 after adenoviral injection (n = 6 per group). *F*: Average daily food intake amounts over the first and the second weeks after adenoviral administration are presented. Regarding all panels, similar results were obtained from 10 or more experiments, and representative results are presented as means ± SE. *P < 0.05, **P < 0.01 assessed by unpaired t test.

cDNA synthesis was performed with a Cloned AMV First Strand Synthesis Kit (Invitrogen, Rockville, MD) using 5 μg of total RNA. cDNA synthesized from total RNA was evaluated in a real-time PCR quantitative system (Light Cycler Quick System 350S; Roche Diagnostics, Mannheim, Germany). The relative amount of mRNA was calculated with glyceraldehyde-3-dehydrogenase mRNA as the invariant control. The primers used are described in Table 1.

All data were expressed as means ± SE. The statistical significance of differences was assessed by the unpaired t test and one-factor ANOVA.

RESULTS

Hepatic UCP1 expression increased energy expenditure and reduced body weight and blood glucose levels in mice that had high-fat diet–induced obesity and diabetes. C57BL/6 mice were on a high-fat diet for 4 weeks, resulting in diabetes associated with obesity. The UCP1 adenovirus vector (11) was then administered intravenously (UCP1 mice). Mice that were given the LacZ adenovirus were used as a control (LacZ mice). No significant alterations were observed in body weights (Fig. 1*B*), blood glucose levels (Fig. 1*C*), food intake amounts, body temperature, or plasma lipid parameters (data not shown) before versus after LacZ adenovirus administration. Systemic infusion of recombinant adenoviruses into mice through the tail vein primarily resulted in expression of transgenes in the liver, with no detectable expression in peripheral tissues such as muscle, fat, kidney, or brain (data not shown), as reported previously (20). As shown in Fig. 1*A*, immunoblotting revealed that ectopic UCP1 expression in the liver peaked on day 3. Maximal expression was maintained through day 8. After day 9, hepatic expression of UCP1 decreased, and very small amounts of UCP1 protein were detected on day 14 (Fig. 1*A*).

In UCP1 mice, body weight and blood glucose levels were markedly decreased (Fig. 1*B* and *C*) concomitantly with hepatic expression levels of UCP1. On day 7, body weights of UCP1 mice were significantly lower, by 13%, than those of control mice. After day 9, body weight and

blood glucose levels began to increase as the expression of hepatic UCP1 declined. These findings indicate that hepatic UCP1 expression exerted therapeutic effects on diabetes associated with diet-induced obesity.

Resting oxygen consumption on day 3 was markedly increased, by 12%, in UCP1 mice compared with controls (Fig. 1*D*), whereas rectal temperature did not differ between the two (Fig. 1*E*). Thus, ectopic UCP1 in the liver, like endogenous UCP1 in brown adipocytes, promoted inefficient metabolism, thereby enhancing energy expenditure and leading to weight reduction. This effect, however, was not sufficient to raise whole-body temperature. In addition, hepatic UCP1 expression changed food intake. Whereas without hepatic UCP1 expression, food intake amounts in high-fat–fed mice were markedly increased compared with those in standard diet–fed lean mice (compare Figs. 1*F* and 5*D*), hepatic UCP1 expression reversed hyperphagia in mice with high-fat diet–induced obesity and diabetes (Fig. 1*F*). After day 8, concomitantly with the drop in hepatic UCP1 expression, hyperphagia was restored (Fig. 1*F*). In contrast, mice received an intravenous injection of adenovirus encoding CPT1a, another mitochondrial protein, did not show significantly altered food consumption (data not shown), suggesting that food intake suppression induced by hepatic UCP1 expression is not a nonspecific effect of expression of any of the hepatic mitochondrial proteins.

To eliminate any secondary effects of reduced food intake induced by hepatic UCP1 expression, we performed pair-feeding experiments. In contrast to UCP1 mice, pair-fed LacZ mice exhibited only slight decreases in body weights and blood glucose levels (of 3.1 and 6.9%, respectively, on day 7 after adenoviral administration). These results suggest that increased energy expenditure is an important mechanism underlying marked improvements of obesity and diabetes in UCP1 mice.

Hepatic UCP1 expression decreased fat contents in the liver and adipose tissues. Hepatic and adipose fat accumulations were examined on day 7 after adenoviral gene delivery. In the high-fat–fed control mice, liver weight and triglyceride content were markedly increased compared with the standard chow–fed lean mice (compare Fig. 2*A* and *B* with Fig. 5*E* and *F*, respectively). Hepatic UCP1 expression significantly decreased liver weight (Fig. 2*A*) and triglyceride content (Fig. 2*B*) compared with LacZ mice, with high-fat feeding. It is interesting that hepatic UCP1 expression also decreased fat content in their adipose tissues. For example, epididymal fat weight was significantly decreased in UCP1 mice compared with that in controls (Fig. 2*C*). Thus, hepatic expression of UCP1 exerts not only local effects in the liver but also remote effects on metabolism in other tissues.

These results were confirmed by the histological findings. No apparent infiltration or structural change was observed in the livers of either LacZ mice or UCP1 mice, indicating the absence of adenovirus-induced liver damage (Fig. 2*D*). Whereas abundant lipid droplets were present in the livers of control mice, these lipid droplets were markedly diminished in UCP1 mouse livers, indicating marked improvement of fatty liver findings in response to UCP1 expression (Fig. 2*D*). Furthermore, the cell diameters in epididymal fat (Fig. 2*E*) and brown adipose (Fig. 2*F*) tissues were significantly decreased in UCP1 mice. Expression levels of endogenous UCP1 protein in brown adipocytes were similar in the two groups (Fig. 2*G*), suggesting that energy expenditure in brown adipocytes was not increased in UCP1 mice. These findings suggest that hepatic UCP1 expression promotes hydrolysis of triglycerides already stored in adipose tissues, leading to smaller adipocytes with the resultant fatty acids being mobilized and metabolized as a substrate for oxidation in the liver.

Hepatic expressions of enzymes involved in lipid metabolism and glucose production. To elucidate the underlying mechanism whereby stored fat was decreased in the liver by hepatic UCP1 expression, we examined the expressions of proteins involved in lipid metabolism by quantitative RT-PCR. Significant reductions in the expressions of the lipogenic enzymes, including stearoyl-CoA desaturase-1 and fatty acid synthase, were observed in UCP1 mice (Fig. 3*A*). Sterol regulatory element binding protein 1c (SREBP1c) expression in the liver tended to be diminished. In contrast, hepatic expressions of enzymes involved in fatty acid oxidation tended to be increased. In particular, expressions of fatty acid transporter and UCP2 were significantly increased (Fig. 3*B*).

We further examined expression levels of key enzymes for hepatic glucose production. Hepatic phosphoenolpyruvate carboxykinase and glucose-6-phosphatase expressions were significantly decreased in UCP1 mice (Fig. 3*C*), suggesting a decrease to contribute to improvement of diabetes.

UCP1 expression may activate AMPK as a result of decreased generation of ATP. AMPK activation reportedly decreases malonyl-CoA generation via inhibition of ACC (21), resulting in enhancement of fatty acid oxidation. Therefore, ATP levels and AMPK phosphorylation in the liver were examined in LacZ and UCP1 mice under ad libitum feeding conditions. Hepatic ATP concentrations in UCP1 mice were approximately half those in control mice (Fig. 3*D*) but still ~2.3-fold those in standard diet–fed control mice. Hepatic AMPK activity was increased 1.6-fold in UCP1 mice compared with LacZ mice (Fig. 3*E*). The phosphorylation state of the α-subunit of AMPK in the liver was enhanced in UCP1 mice (Fig. 3*F*). Furthermore, resultant enhancement of hepatic ACC phosphorylation was observed (Fig. 3*G*). These findings suggest that AMPK activation induced by UCP1 expression plays an important role in the observed marked improvement of fatty liver findings via enhanced fatty acid oxidation.

Glucose and lipid metabolism in UCP1 mice. The results of oral glucose tolerance (Fig. 4*A*) and insulin tolerance (Fig. 4*B*) tests on day 7 after adenoviral administration clearly showed that hepatic expression of UCP1 markedly improved glucose tolerance and insulin sensitivity in obese and diabetic mice. Improved insulin sensitivity in muscle was confirmed by enhanced insulin receptor and IRS1 phosphorylation (Fig. 4*C*) in response to insulin administration. Thus, hepatic UCP1 expression exerts a remote beneficial effect on insulin sensitivity in muscle.

In addition, plasma lipid parameters were decreased in UCP1 mice. Total plasma cholesterol levels tended to be decreased in UCP1 mice compared with controls, although the changes were not statistically significant (Fig. 4*D*). Plasma triglyceride and free fatty acid levels were signifi-

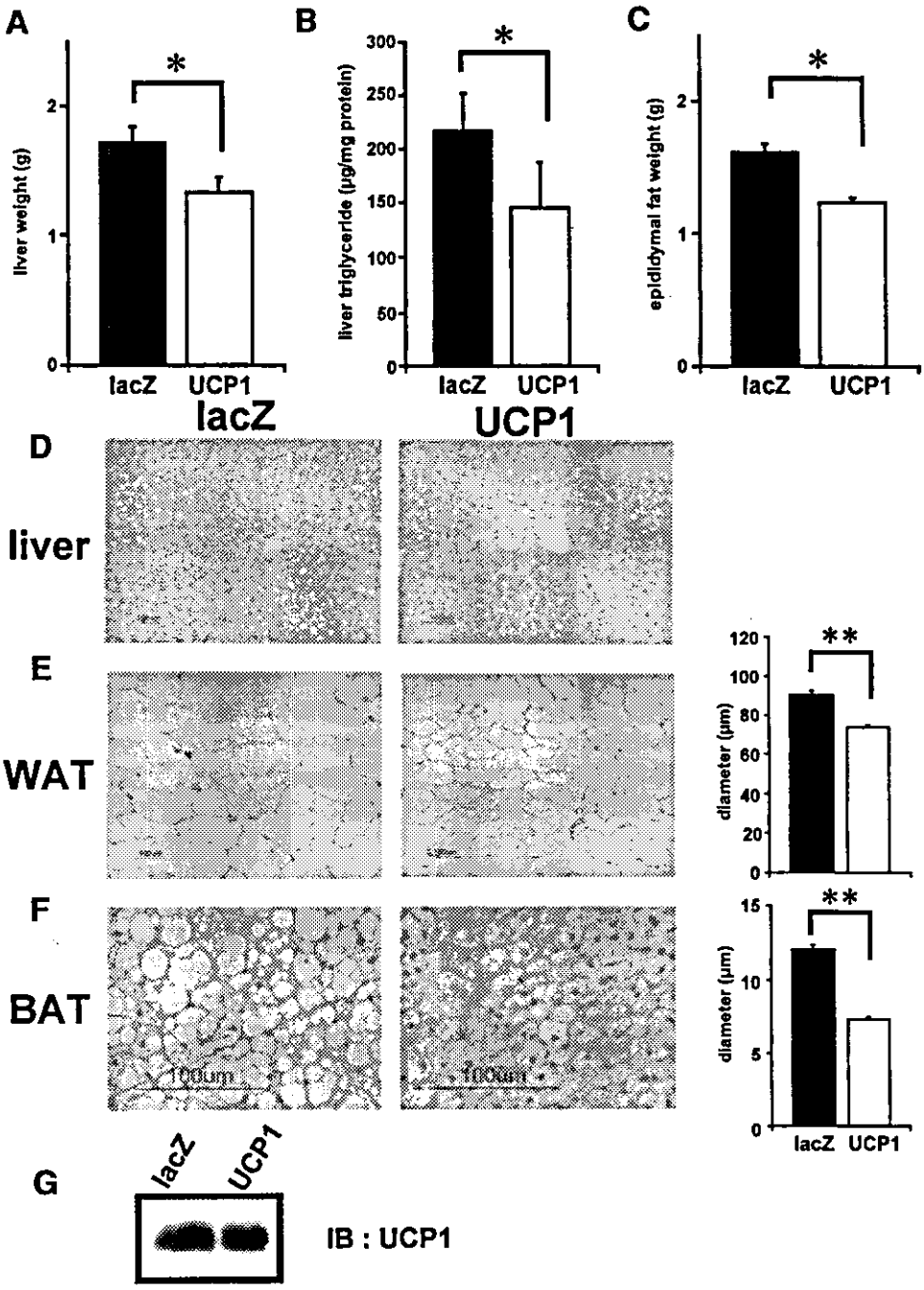

FIG. 2. Hepatic and adipose fat accumulations were decreased in UCP1 mice. Mice were killed after a 10-h fast on day 7 after adenoviral injection, and liver, epididymal fat (WAT), and brown adipose tissues (BAT) were removed. Liver weight (*A*), triglyceride content (*B*), and epididymal fat weight (*C*) were determined (n = 6 per group). *D–F*: Histological findings with hematoxylin and eosin (HE) staining of the liver (*D*), WAT (*E*), and BAT (*F*) in high-fat–fed control (*left*) and UCP1 mice (*middle*). In WAT (*E*) and BAT (*F*) tissues, cell diameters were measured (*right*). *G*: Endogenous UCP1 expression in BAT was compared between control (*left lane*) and UCP1 mice (*right lane*) by immunoblotting (n = 6 per group). Representative histological findings and immunoblots are presented. Data are presented as means ± SE. *P < 0.05, **P < 0.01 assessed by unpaired t test.

cantly decreased in UCP1 mice (Fig. 4*D*). Thus, hepatic UCP1 expression also improved diet-induced dyslipidemia.

Serum insulin levels were markedly decreased, by 57% (Fig. 4*E*), in UCP1 mice, despite lower blood glucose levels (Fig. 1*C*), indicating marked improvement of systemic insulin sensitivity. Serum adiponectin and TNF-α levels were similar in these groups (Fig. 4*F*), suggesting that these adipocytokines are not involved in the improvement of insulin resistance in UCP1 mice. In contrast, serum leptin levels were significantly decreased, by 56%, in

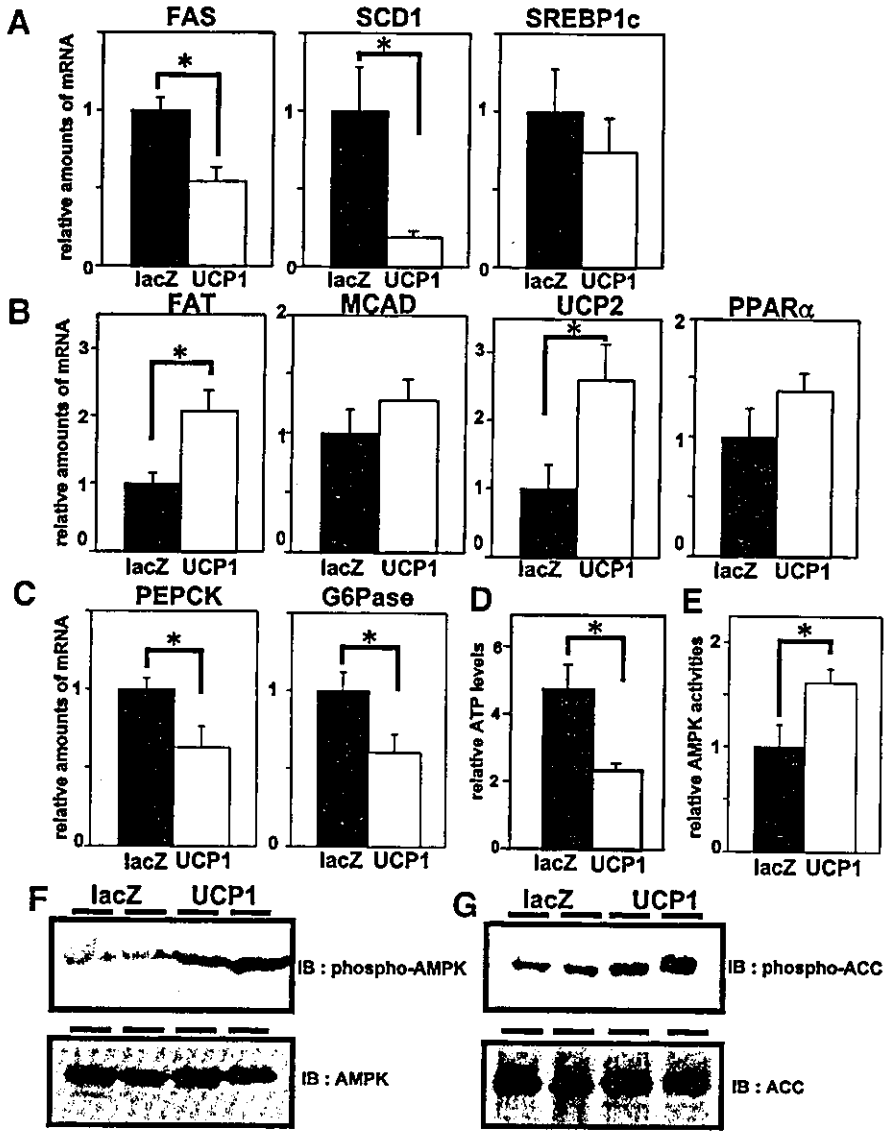

FIG. 3. Hepatic expressions of enzymes involved in lipid metabolism and glucose production and phosphorylations of AMPK and ACC. *A–C*: Relative amounts of mRNA were measured by quantitative RT-PCR and corrected with glyceraldehyde-3-dehydrogenase as the standard. Hepatic total RNA of mice, on day 3 after adenoviral administration in the 10-h–fasted state, was isolated. Expressions of lipogenic enzymes and SREBP1c (*A*), enzymes for fatty acid oxidation and PPAR-α (*B*), and enzymes for hepatic glucose production (*C*) in the liver were assayed (n = 6 per group). *D* and *E*: ATP concentrations (*D*) and AMPK activity (*E*) in the liver were measured. Data are presented as the relative amounts compared with those in standard diet–fed control mice (n = 6 per group). *F* and *G*: Immunoblots using anti–phospho-AMPK (*F*) or anti–phospho-ACC (*G*) antibody (*top*), as well as anti-AMPK (*F*) or anti-ACC1 (*G*) antibody (*bottom*) revealed the phosphorylation state of the AMPK α-subunit in the liver on day 3 after adenoviral injection (n = 2 per group). Data are presented as means ± SE. *P < 0.05 assessed by unpaired t test.

UCP1 mice compared with those in control mice (Fig. 4*F*) concomitantly with decreased food intake (Fig. 1*F*). In control mice that were fed a high-fat diet, marked hyperleptinemia was observed (serum leptin concentrations, standard diet–fed mice versus high-fat diet–fed mice: 0.48 ± 0.08 vs. 32 0.8 ± 4.6 ng/ml) despite increased food intake (compare Fig. 1*F* with Fig. 5*D*), indicating leptin resistance. The present results suggest that hepatic UCP1 expression improves hypothalamic leptin resistance in obese and diabetic mice. To directly test whether leptin sensitivity was improved, we performed leptin tolerance tests (Fig. 4*G*). Leptin was injected intraperitoneally into fasted mice, followed by measurement of 12-h food intakes. The food intake inhibition by leptin administration was far more profound in UCP1 mice than in LacZ mice. Thus, UCP1 mice responded strongly to leptin administration, clearly showing that hepatic UCP1 expression exerts a therapeutic effect on hypothalamic leptin resistance.

Hepatic UCP1 expression exerted minimal effects in standard diet–fed lean mice. Hepatic UCP1 expression reduced body weight and blood glucose and lipid levels in obese and diabetic mice. These are very promising results suggesting that ectopic UCP1 expression may be useful in treating diabetic individuals who are obese. However, if

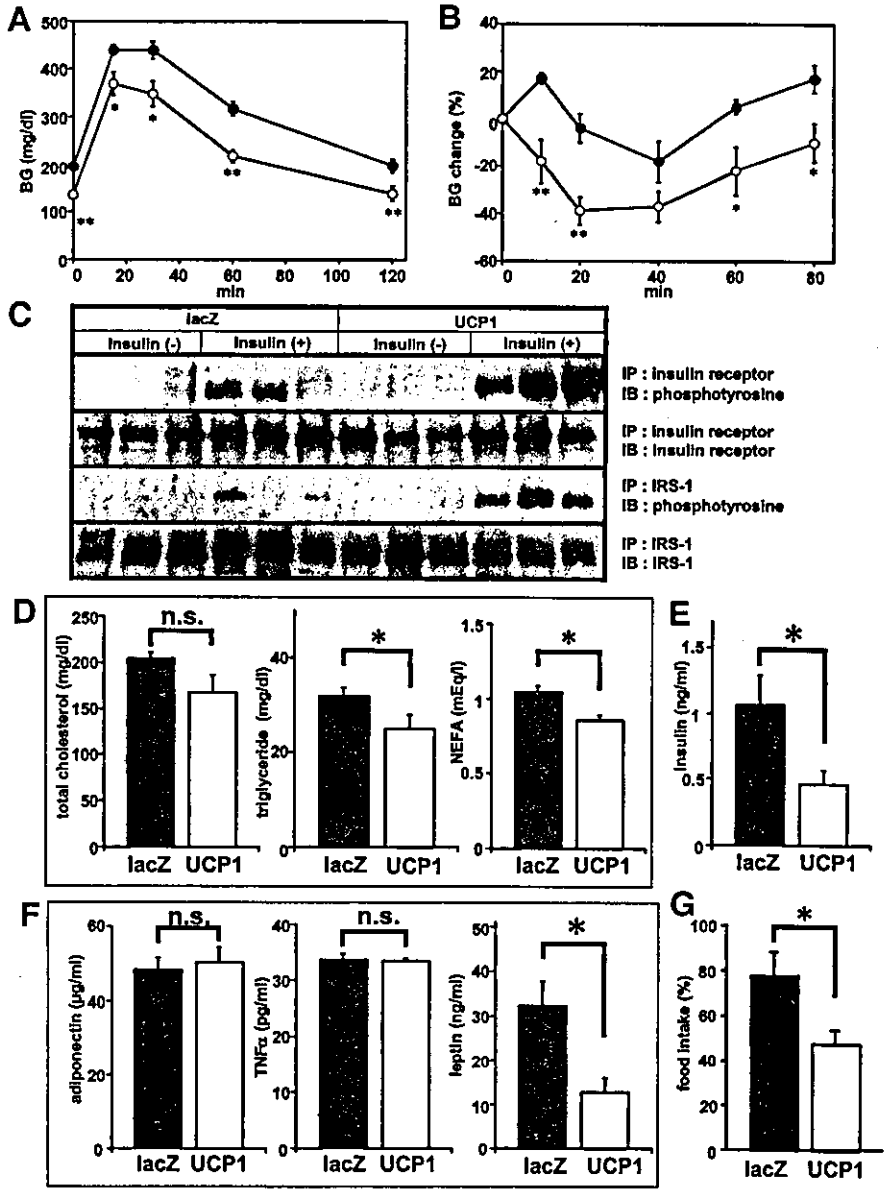

FIG. 4. Hepatic UCP1 expression improved glucose tolerance and insulin sensitivity. *A* and *B*: High-fat–fed mice on day 7 after adenoviral administration were subjected to glucose tolerance (*A*) and insulin tolerance (*B*) tests. Glucose tolerance tests were performed with an oral glucose load (2 g/kg body wt) after a 10-h fast. Insulin tolerance tests were performed in an ad libitum–fed state. Data were expressed as percentages of blood glucose levels immediately before intraperitoneal insulin loading (0.75 units/kg body wt). *C*: Insulin-stimulated tyrosine phosphorylation of insulin receptor and IRS1 proteins in muscle (n = 3 per group). Mice that were fasted for 16 h received an intravenous injection of 100 μl of normal saline with or without insulin (10 units/kg body wt). Hindlimb muscles were removed 300 s later, and lysates were immunoprecipitated with each antibody, as indicated. Immunoprecipitates were subjected to SDS-PAGE and immunoblotted with anti-phosphotyrosine antibody (4G10) or individual antibodies as indicated. *D–F*: Plasma lipid parameters (*D*; *left*, total cholesterol; *middle*, triglyceride; *right*, free fatty acids), serum insulin (*E*), and adipocytokines (*F*; *left*, adiponectin; *middle*, TNF-α; *right*, leptin) of high-fat–fed mice on day 7 after adenoviral administration were measured in the 10-h–fasted state. *G*: Leptin tolerance tests were performed on day 7 after adenoviral administration as described in RESEARCH DESIGN AND METHODS. Data were expressed as ratios to the food intake amounts of vehicle-treated mice (n = 6 per group). Data are presented as means ± SE. *P < 0.05, **P < 0.01 assessed by unpaired t test.

this were also the case in lean individuals, then these individuals would become leaner, possibly even developing malnutrition and hypoglycemia. We therefore performed experiments with a similar design but used 9-week-old standard diet–fed lean mice, i.e., the same age as the high-fat–fed mice.

It is intriguing that although ectopic UCP1 expression levels in the liver were similar under high-fat and standard diet conditions (Fig. 5*A*), the resultant phenotypes were completely different. In standard diet–fed lean mice, hepatic UCP1 expression did not alter body weight (Fig. 5*B*), fasting blood glucose levels (Fig. 5*C*), or food intake

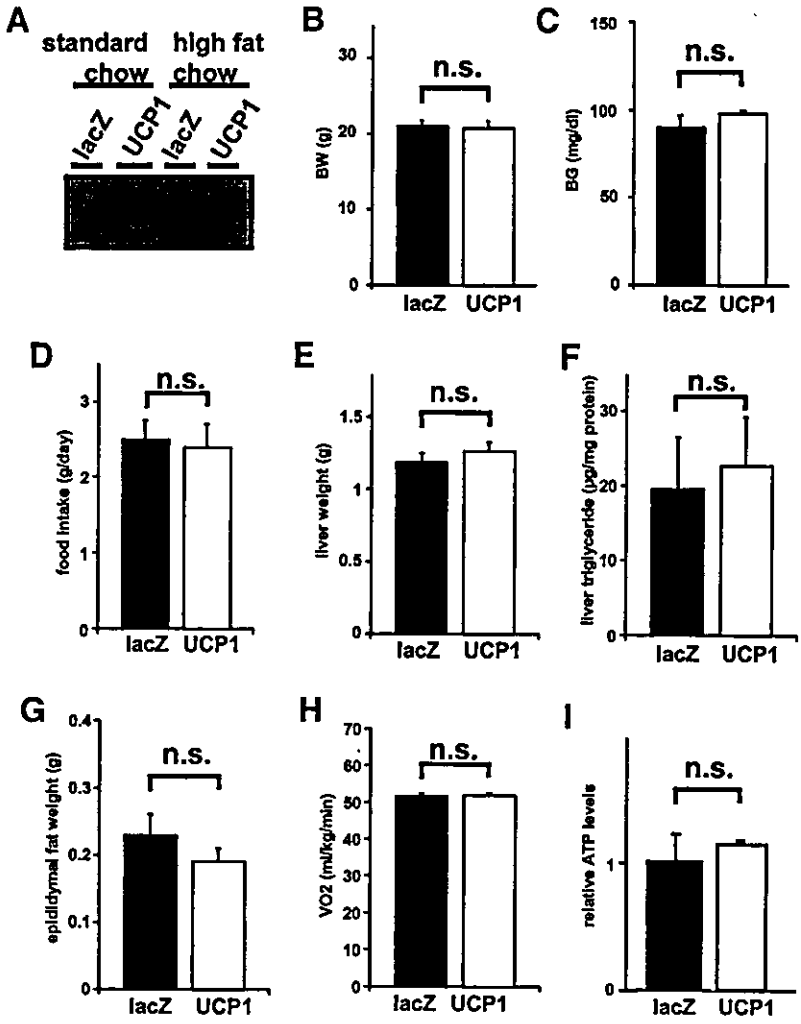

FIG. 5. Minimal effects of hepatic UCP1 expression in standard diet–fed lean mice. *A*: Hepatic UCP1 expression in standard or high-fat diet–fed mice on day 7 after adenoviral administration at 9 weeks of age. Liver extracts from mice were immunoblotted using anti-UCP1 antibody. *B* and *C*: Body weights (*B*) and fasting blood glucose levels (*C*) were measured on day 7 after adenoviral injection. *D*: Food intake amounts were measured daily, and the average daily food intake for 7 days after adenoviral administration is represented. *E–G*: Hepatic weights (*E*), triglyceride contents (*F*), and epididymal fat weights (*G*) were determined (n = 6 per group) on day 7 after adenoviral injection. *H* and *I*: Resting Vo_2 (*H*) and hepatic ATP levels (*I*) were measured in the same way as in previous figures. Hepatic ATP levels are presented as the relative amounts compared with those in standard diet–fed control mice. Data are presented as means ± SE. $^{**}P < 0.01$ assessed by one-factor ANOVA.

amounts (Fig. 5*D*). In addition, hepatic weight (Fig. 5*E*), triglyceride content (Fig. 5*F*), and epididymal fat weight (Fig. 5*G*) were not changed. Thus, hepatic UCP1 expression did not exert significant effects on glucose metabolism or adiposity in lean mice.

To determine why hepatic UCP1 expression in lean mice did not significantly alter metabolic conditions, we measured basal energy expenditure and hepatic ATP contents. Hepatic UCP1 expression did not significantly change basal energy expenditure (Fig. 5*H*) or hepatic ATP levels (Fig. 5*I*), suggesting that UCP1 ectopically expressed in the liver is minimally involved in mitochondrial uncoupling, when surplus energy is not stored in the liver. Thus, hepatic UCP1 is likely to dissipate excess energy while having no effect on required energy. These characteristics are favorable in terms of therapeutic strategies for the metabolic syndrome.

DISCUSSION

In this study, after mice had developed obesity-associated diabetes, ectopically expressing UCP1 in the liver resulted in marked improvements in both disease conditions. UCP1 expression would be expected to decrease ATP generation in the liver and thus to activate hepatic AMPK. Indeed, ATP contents were decreased, and AMPK and ACC phosphorylations were increased. AMPK reportedly phosphorylates and inactivates ACC, resulting in a decrease in malonyl-CoA generation (21). Because malonyl-CoA is a negative regulator via suppression of CPT1, a rate-limiting enzyme for fatty acid oxidation (22), a decrease in malonyl-CoA generation is likely to enhance fatty acid oxidation to meet respiratory demands. Furthermore, hepatic expressions of lipogenic enzymes were decreased by UCP1 expression in the liver, which may be explained by

AMPK activation and possible SREBP1 reduction in the liver; metformin reportedly activates AMPK and inhibits hepatic SREBP1 expression (23). Taken together, the results suggest that fatty acid synthesis was suppressed with concomitant enhancement of fatty acid oxidation, resulting in the marked decrease in hepatic triglyceride contents.

How might a change in hepatic lipid metabolism affect the energy balance of the entire body? It is noteworthy that the weight and/or cell sizes of epididymal fat and brown adipose tissues were markedly decreased by hepatic UCP1 expression in the present study. Inhibition of fat accumulation in adipose tissues was also observed in UCP1 and in UCP3 transgenic mice under the control of muscle-specific promoters (7,8). Mice lacking ACC2, which is predominantly expressed in the heart and muscle of wild-type mice, also markedly inhibited fat accumulation in their adipose tissues (24). In reports using transgenic models, muscle is a site of increasing energy expenditure, through mitochondrial uncoupling, which prevents obesity. In the present study, hepatic expression of UCP1 reduced fat contents, rather than inhibiting fat accumulation, not only in the liver but also in adipose tissues, indicating promotion of hydrolysis of triglycerides already stored in the adipose tissues. Thus, hepatic uncoupling is likely to convey signals to peripheral adipose tissues. These signals might involve an autonomic nerve network, because the hydrolysis of triglycerides stored in adipose tissues is controlled mainly by the cAMP-mediated pathway, including sympathetic nerve activation (25). Alternatively, a decline in serum fatty acid concentrations, observed in UCP1 mice, or some unknown factors secreted by the liver might trigger lipolysis in adipose tissues. Although more work is required to elucidate the mechanism underlying this remote effect, enhancement of hepatic uncoupling is likely to exert therapeutic, rather than preventive, effects on insulin resistance associated with obesity. Thus, the liver is a potential therapeutic target for diabetes with obesity. Furthermore, unraveling the underlying mechanism may lead to development of antiobesity pharmacological agents that promote lipolysis in adipose tissues.

The present results are also interesting with respect to appetite regulation. Transgenic mice overexpressing UCP3 in skeletal muscle are reportedly hyperphagic (8), whereas UCP1 transgenic mice show no changes in food intake (7). In these transgenic mice, UCPs are continuously overexpressed throughout life, including in the fetal stage. In contrast, the UCP was expressed after development of diabetes with obesity in the present study. In obese subjects, serum leptin levels are reportedly increased with an increment in adipose tissue mass (26,27). Despite increased serum leptin levels, neither appetite nor food intake was suppressed, but instead increased, which is explained by hypothalamic leptin resistance in obese subjects. Herein, control mice on a high-fat diet were hyperphagic compared with those on a standard diet, whereas serum leptin levels were markedly elevated in high-fat diet–fed mice, indicating the development of leptin resistance. It is interesting that hepatic UCP1 expression reversed hyperphagia in high-fat diet–fed mice. Leptin tolerance tests show marked improvement of hypothalamic leptin resistance in UCP1 mice, another remote effect of hepatic UCP1 expression. In addition, increased fatty acid oxidation might be involved in the decreased food intake, because administration of peroxisome proliferator–activated receptor (PPAR)-α agonists reportedly reduces food intake amounts, but not in mice deficient in PPAR-α (28). Furthermore, streptozotocin-induced hyperphagia was reportedly reversed by hepatic expression of protein phosphatase-1 (29), suggesting that altering hepatic metabolism modulates appetite. Vagal pathways from the liver to the brain mediate the fat-induced changes in hypothalamic neuropeptides and feeding behavior in diabetic rats (30). Taken together with these observations, through appetite modulation, the liver also holds promise as a target for treatment of diabetes with obesity.

The most intriguing finding of the present study is that, despite similar UCP1 expression levels in mice on high-fat and standard diets, the resultant phenotypes were completely different. Hepatic UCP1 expression exerted no significant effects on food intake, weight change, or blood glucose levels in standard diet–fed lean mice. No alterations in energy expenditure or hepatic ATP contents were observed with hepatic UCP1 expression, indicating that, in the absence of a significant energy surplus, ectopic UCP1 has minimal effects on mitochondrial uncoupling. We performed similar experiments in a mildly obese and insulin-resistant model, 15% fat-fed mice. In these mice, hepatic UCP1 expression did not change body weight or food intake. Glucose tolerance and insulin sensitivity were significantly improved, but the effects were smaller (data not shown) than those in a more severely obese and insulin-resistant model, 32% fat-fed mice, reported here. Furthermore, under 32% high-fat–fed conditions in the present study, although hepatic UCP1 expression decreased ATP levels in the liver, the reduced ATP concentrations still exceeded those in standard diet–fed mice, suggesting that enhanced expression of UCPs in the liver does not itself produce an energy shortage. Taken together, hepatic UCP1 is likely to sense the metabolic state in the liver and function according to the degree of stored energy in the liver. In the reconstituted system, addition of fatty acids is indispensable for proton transport by UCP1 (31,32). Although the underlying mechanism has been widely debated (33,34), fatty acid cycling seems to be important for proton transport by UCP1 (35,36). Via such a mechanism, ectopic UCP1 activity in the liver may depend on the metabolic state, probably on the amount of stored fat in the liver. Thus, hepatic UCP1 seems to dissipate surplus energy but not to affect required energy. Therefore, the liver, in which intracellularly stored fat changes dramatically according to the energy balance, seems to be a good target tissue for enhanced expression of UCPs. This feature is of particular importance, as applied to therapeutic strategies for type 2 diabetes associated with obesity and insulin resistance.

Recently, it was reported that, using a transgenic technique, skeletal muscle expression of UCP1 in genetically obese mice lowers blood pressure (37), suggesting that uncoupling decreases the risk for atherosclerosis in patients with obesity and type 2 diabetes. In addition, uncoupling reportedly decreases the production of reactive oxygen species (38), although total oxygen consumption

increases. A high mitochondrial electrochemical gradient is associated with the production of reactive oxygen species that may damage tissues, a possible cause of diabetes complications and atherosclerosis (39). Thus, the respiratory uncoupling increment in the liver may protect tissues from oxidative stress. Taken together with the results of the present study, enhancement of UCPs in the liver is a potential therapy for the metabolic syndrome via reductions in adiposity and blood glucose levels as well as possibly reactive oxygen species in obese and diabetic individuals.

ACKNOWLEDGMENTS

This work was supported by a Grant-in-Aid for Scientific Research (B2, 15390282); a Grant-in-Aid for Exploratory Research (15659214); and Tohoku University 21st Century COE Program "Comprehensive Research and Education Center for Planning of Drug Development and Clinical Evaluation" to H.K. and a Grant-in-Aid for Scientific Research (13204062); and Tohoku University 21st Century COE Program "the Center for Innovative Therapeutic Development for Common Diseases" to Y.O. from the Ministry of Education, Science, Sports and Culture of Japan.

We thank Prof. Y. Moriyama (Okayama University) for helpful suggestions for measuring ATP. We also thank I. Sato and K. Kawamura for technical support.

REFERENCES

1. Friedman JM: A war on obesity, not the obese. *Science* 299:856–858, 2003
2. Klingenberg M, Huang SG: Structure and function of the uncoupling protein from brown adipose tissue. *Biochim Biophys Acta* 1415:271–296, 1999
3. Enerback S, Jacobsson A, Simpson EM, Guerra C, Yamashita H, Harper ME, Kozak LP: Mice lacking mitochondrial uncoupling protein are cold-sensitive but not obese. *Nature* 387:90–94, 1997
4. Himms-Hagen J: Brown adipose tissue thermogenesis and obesity. *Prog Lipid Res* 28:67–115, 1989
5. Kopecky J, Clarke G, Enerback S, Spiegelman B, Kozak LP: Expression of the mitochondrial uncoupling protein gene from the aP2 gene promoter prevents genetic obesity. *J Clin Invest* 96:2914–2923, 1995
6. Kopecky J, Hodny Z, Rossmeisl M, Syrovy I, Kozak LP: Reduction of dietary obesity in aP2-Ucp transgenic mice: physiology and adipose tissue distribution. *Am J Physiol* 270:E768–E775, 1996
7. Li B, Nolte LA, Ju JS, Han DH, Coleman T, Holloszy JO, Semenkovich CF: Skeletal muscle respiratory uncoupling prevents diet-induced obesity and insulin resistance in mice. *Nat Med* 6:1115–1120, 2000
8. Clapham JC, Arch JR, Chapman H, Haynes A, Lister C, Moore GB, Piercy V, Carter SA, Lehner I, Smith SA, Beeley LJ, Godden RJ, Herrity N, Skehel M, Changani KK, Hockings PD, Reid DG, Squires SM, Hatcher J, Trail B, Latcham J, Rastan S, Harper AJ, Cadenas S, Buckingham JA, Brand MD, Abuin A: Mice overexpressing human uncoupling protein-3 in skeletal muscle are hyperphagic and lean. *Nature* 406:415–418, 2000
9. Ono H, Shimano H, Katagiri H, Yahagi N, Sakoda H, Onishi Y, Anai M, Ogihara T, Fujishiro M, Viana AY, Fukushima Y, Abe M, Shojima N, Kikuchi M, Yamada N, Oka Y, Asano T: Hepatic Akt activation induces marked hypoglycemia, hepatomegaly, and hypertriglyceridemia with sterol regulatory element binding protein involvement. *Diabetes* 52:2905–2913, 2003
10. Kozak LP, Britton JH, Kozak UC, Wells JM: The mitochondrial uncoupling protein gene: correlation of exon structure to transmembrane domains. *J Biol Chem* 263:12274–12277, 1988
11. Nakazaki M, Kakei M, Ishihara H, Koriyama N, Hashiguchi H, Aso K, Fukudome M, Oka Y, Yada T, Tei C: Association of upregulated activity of K(ATP) channels with impaired insulin secretion in UCP1-expressing insulinoma cells. *J Physiol* 540:781–789, 2002
12. Katagiri H, Asano T, Ishihara H, Inukai K, Shibasaki Y, Kikuchi M, Yazaki Y, Oka Y: Overexpression of catalytic subunit p110α of phosphatidylinositol 3-kinase increases glucose transport activity with translocation of glucose transporters in 3T3–L1 adipocytes. *J Biol Chem* 271:16987–16990, 1996
13. Kanegae Y, Lee G, Sato Y, Tanaka M, Nakai M, Sakaki T, Sugano S, Saito I: Efficient gene activation in mammalian cells by using recombinant adenovirus expressing site-specific Cre recombinase. *Nucleic Acids Res* 23:3816–3821, 1995
14. Ikemoto S, Thompson KS, Takahashi M, Itakura H, Lane MD, Ezaki O: High fat diet-induced hyperglycemia: prevention by low level expression of a glucose transporter (GLUT4) minigene in transgenic mice. *Proc Natl Acad Sci U S A* 92:3096–3099, 1995
15. Ogihara T, Shin BC, Anai M, Katagiri H, Inukai K, Funaki M, Fukushima Y, Ishihara H, Takata K, Kikuchi M, Yazaki Y, Oka Y, Asano T: Insulin receptor substrate (IRS)-2 is dephosphorylated more rapidly than IRS-1 via its association with phosphatidylinositol 3-kinase in skeletal muscle cells. *J Biol Chem* 272:12868–12873, 1997
16. Folch J, Lees M, Sloane Stanley GH: A simple method for the isolation and purification of total lipides from animal tissues. *J Biol Chem* 226:497–509, 1957
17. Manfredi G, Yang L, Gajewski CD, Mattiazzi M: Measurements of ATP in mammalian cells. *Methods* 26:317–326, 2002
18. Sakoda H, Ogihara T, Anai M, Fujishiro M, Ono H, Onishi Y, Katagiri H, Abe M, Fukushima Y, Shojima N, Inukai K, Kikuchi M, Oka Y, Asano T: Activation of AMPK is essential for AICAR-induced glucose uptake by skeletal muscle but not adipocytes. *Am J Physiol Endocrinol Metab* 282:E1239–E1244, 2002
19. Igel M, Becker W, Herberg L, Joost HG: Hyperleptinemia, leptin resistance, and polymorphic leptin receptor in the New Zealand obese mouse. *Endocrinology* 138:4234–4239, 1997
20. Ishigaki Y, Oikawa S, Suzuki T, Usui S, Magoori K, Kim DH, Suzuki H, Sasaki J, Sasano H, Okazaki M, Toyota T, Saito T, Yamamoto TT: Virus-mediated transduction of apolipoprotein E (ApoE)-sendai develops lipoprotein glomerulopathy in ApoE-deficient mice. *J Biol Chem* 275: 31269–31273, 2000
21. Hardie DG: Regulation of fatty acid and cholesterol metabolism by the AMP-activated protein kinase. *Biochim Biophys Acta* 1123:231–238, 1992
22. McGarry JD, Brown NF: The mitochondrial carnitine palmitoyltransferase system: from concept to molecular analysis. *Eur J Biochem* 244:1–14, 1997
23. Zhou G, Myers R, Li Y, Chen Y, Shen X, Fenyk-Melody J, Wu M, Ventre J, Doebber T, Fujii N, Musi N, Hirshman MF, Goodyear LJ, Moller DE: Role of AMP-activated protein kinase in mechanism of metformin action. *J Clin Invest* 108:1167–1174, 2001
24. Abu-Elheiga L, Matzuk MM, Abo-Hashema KA, Wakil SJ: Continuous fatty acid oxidation and reduced fat storage in mice lacking acetyl-CoA carboxylase 2. *Science* 291:2613–2616, 2001
25. Londos C, Brasaemle DL, Schultz CJ, Adler-Wailes DC, Levin DM, Kimmel AR, Rondinone CM: On the control of lipolysis in adipocytes. *Ann N Y Acad Sci* 892:155–168, 1999
26. Maffei M, Halaas J, Ravussin E, Pratley RE, Lee GH, Zhang Y, Fei H, Kim S, Lallone R, Ranganathan S, et al.: Leptin levels in human and rodent: measurement of plasma leptin and ob RNA in obese and weight-reduced subjects. *Nat Med* 1:1155–1161, 1995
27. Considine RV, Sinha MK, Heiman ML, Kriauciunas A, Stephens TW, Nyce MR, Ohannesian JP, Marco CC, McKee LJ, Bauer TL, et al.: Serum immunoreactive-leptin concentrations in normal-weight and obese humans. *N Engl J Med* 334:292–295, 1996
28. Fu J, Gaetani S, Oveisi F, Lo Verme J, Serrano A, Rodriguez De Fonseca F, Rosengarth A, Luecke H, Di Giacomo B, Tarzia G, Piomelli D: Oleylethanolamide regulates feeding and body weight through activation of the nuclear receptor PPAR-alpha. *Nature* 425:90–93, 2003
29. Yang R, Newgard CB: Hepatic expression of a targeting subunit of protein phosphatase-1 in streptozotocin-diabetic rats reverses hyperglycemia and hyperphagia despite depressed glucokinase expression. *J Biol Chem* 278:23418–23425, 2003
30. la Fleur SE, Ji H, Manalo SL, Friedman MI, Dallman MF: The hepatic vagus mediates fat-induced inhibition of diabetic hyperphagia. *Diabetes* 52:2321–2330, 2003
31. Strieleman PJ, Schalinske KL, Shrago E: Fatty acid activation of the reconstituted brown adipose tissue mitochondria uncoupling protein. *J Biol Chem* 260:13402–13405, 1985
32. Winkler E, Klingenberg M: Effect of fatty acids on H+ transport activity of the reconstituted uncoupling protein. *J Biol Chem* 269:2508–2515, 1994
33. Klingenberg M, Echtay KS: Uncoupling proteins: the issues from a biochemist point of view. *Biochim Biophys Acta* 1504:128–143, 2001

34. Jezek P: Possible physiological roles of mitochondrial uncoupling proteins—UCPn. *Int J Biochem Cell Biol* 34:1190–1206, 2002
35. Skulachev VP: Fatty acid circuit as a physiological mechanism of uncoupling of oxidative phosphorylation. *FEBS Lett* 294:158–162, 1991
36. Garlid KD, Orosz DE, Modriansky M, Vassanelli S, Jezek P: On the mechanism of fatty acid-induced proton transport by mitochondrial uncoupling protein. *J Biol Chem* 271:2615–2620, 1996
37. Bernal-Mizrachi C, Weng S, Li B, Nolte LA, Feng C, Coleman T, Holloszy JO, Semenkovich CF: Respiratory uncoupling lowers blood pressure through a leptin-dependent mechanism in genetically obese mice. *Arterioscler Thromb Vasc Biol* 22:961–968, 2002
38. Vidal-Puig AJ, Grujic D, Zhang CY, Hagen T, Boss O, Ido Y, Szczepanik A, Wade J, Mootha V, Cortright R, Muoio DM, Lowell BB: Energy metabolism in uncoupling protein 3 gene knockout mice. *J Biol Chem* 275:16258–16266, 2000
39. Esposito LA, Melov S, Panov A, Cottrell BA, Wallace DC: Mitochondrial disease in mouse results in increased oxidative stress. *Proc Natl Acad Sci U S A* 96:4820–4825, 1999

Available online at www.sciencedirect.com
SCIENCE DIRECT®
Biochemical and Biophysical Research Communications 326 (2005) 402–409
BBRC
www.elsevier.com/locate/ybbrc

Constitutively active PDX1 induced efficient insulin production in adult murine liver

Junta Imai[a,b], Hideki Katagiri[b,*], Tetsuya Yamada[a], Yasushi Ishigaki[a], Takehide Ogihara[b], Kenji Uno[a,b], Yutaka Hasegawa[a,b], Junhong Gao[a,b], Hisamitsu Ishihara[a], Hironobu Sasano[c], Hiroyuki Mizuguchi[d], Tomoichiro Asano[e], Yoshitomo Oka[a]

[a] *Division of Molecular Metabolism and Diabetes, Tohoku University Graduate School of Medicine, Japan*
[b] *Division of Advanced Therapeutics for Metabolic Diseases, Center for Translational and Advanced Animal Research, Tohoku University Graduate School of Medicine, Japan*
[c] *Division of Anatomic Pathology, Tohoku University Graduate School of Medicine, Sendai 980-8575, Japan*
[d] *Division of Cellular and Gene Therapy Products, National Institute of Health Science, Tokyo, Japan*
[e] *Department of Physiological Chemistry and Metabolism, University of Tokyo, Tokyo 113-8655, Japan*

Received 21 October 2004
Available online 19 November 2004

Abstract

To generate insulin-producing cells in the liver, recombinant adenovirus containing a constitutively active mutant of PDX1 (PDX1-VP16), designed to activate target genes without the need for protein partners, was prepared and administered intravenously to streptozotocin (STZ)-treated diabetic mice. The effects were compared with those of administering wild-type PDX1 (wt-PDX1) adenovirus. Administration of these adenoviruses at 2×10^8 pfu induced similar levels of PDX1 protein expression in the liver. While wt-PDX1 expression exerted small effects on blood glucose levels, treatment with PDX1-VP16 adenovirus efficiently induced insulin production in hepatocytes, resulting in reversal of STZ-induced hyperglycemia. The effects were sustained through day 40 when exogenous PDX1-VP16 protein expression was undetectable in the liver. Endogenous PDX1 protein came to be expressed in the liver, which is likely to be the mechanism underlying the sustained effects. On the other hand, albumin and transferrin expressions were observed in insulin-producing cells in the liver, suggesting preservation of hepatocytic functions. Thus, transient expression of an active mutant of PDX1 in the liver induced sustained PDX1 and insulin expressions without loss of hepatocytic function.

Keywords: Insulin; PDX1; Gene therapy; Diabetes; Adenovirus; Transdifferentiation

Type 1 diabetes mellitus is characterized by progressive loss of pancreatic β cells, leading to a lifelong dependency on insulin treatments. Recently, marked advances have been made in transplanting pancreatic islets from human cadavers into type 1 diabetics [1]. However, immune rejection and donor supply are still major challenges in islet cell transplantation. In this context, generation of insulin-producing cells by somatic gene therapy may represent a viable alternative for the treatment for diabetes.

The liver is a possible target organ for generation of insulin-producing cells. Pancreatic and hepatic tissues both express several transcription factors such as HNF1α and C/EBPβ. In addition, these tissues also have similar glucose sensing machinery consisting of the GLUT2 glucose transporter and glucokinase. Furthermore, during embryogenesis, the liver and the ventral pancreas appear to arise from the same cell

* Corresponding author. Fax: +81 22 717 8228.
E-mail address: katagiri-tky@umin.ac.jp (H. Katagiri).

0006-291X/$ - see front matter © 2004 Elsevier Inc. All rights reserved.
doi:10.1016/j.bbrc.2004.11.047

population located within the embryonic endoderm [2]. The gene most likely to be responsible for the difference between the liver and pancreas is pancreatic and duodenal homeobox gene 1 (PDX1), also known as IDX1/IPF1/STF1. PDX1 is expressed in pancreatic buds in the endoderm prior to morphological development of the pancreas [3,4] and has been shown to play a fundamental role in regulating pancreatic development. Gene disruption of PDX1 has been shown to inhibit pancreatic bud maturation and outgrowth, resulting in complete absence of the pancreas [5]. In addition, conditional inactivation of PDX1 in insulin-producing cells results in a progressive loss of β cells, suggesting PDX1 to play an essential role in maintaining β cells [6].

Therefore, to generate insulin-producing cells, several groups have overexpressed PDX1 in various sites [7–11]. Adenovirus-mediated transfer of the PDX1 gene reportedly ameliorates streptozotocin (STZ)-induced hyperglycemia in a short time (within 10 days) [7] as well as for longer periods [12] via production of insulin in the liver. However, helper-dependent adenovirus (HDAD)-mediated PDX1 gene transfer into the liver reportedly results in severe hepatitis and functional failure due to production of pancreatic exocrine enzymes [10]. In addition, transgenic mice overexpressing PDX1 in the liver also develop liver failure [11].

PDX1 has been shown to activate target genes by association with several co-factors such as PBX [13] and the expressions of these protein partners are absent in the liver. To produce a version of PDX1 that would activate target genes without the need for protein partners, the VP16 activation domain from herpes simplex virus was fused to the C-terminus of PDX1 (PDX1-VP16). In PDX1-VP16 transgenic *Xenopus* tadpoles, part or all of the liver is converted to pancreatic tissue, while hepatic differentiation products are lost from the regions converted to pancreas [14].

Therefore, in the present study, we prepared PDX1-VP16 adenovirus and compared the effects of PDX1-VP16 expression with those of wt-PDX1 in the adult murine liver in vivo. These recombinant adenoviruses were administered at a titer of 2×10^8 pfu, which is one to two orders of magnitude lower than those used in previous reports [7,12]. Herein we demonstrate PDX1-VP16 gene transduction to induce hepatocytic production of insulin, but not glucagon or amylase, more efficiently than wt-PDX1, resulting in reversal of STZ-induced hyperglycemia. We found that PDX1-VP16 gene therapy induced endogenous PDX1 expression in the liver, and hence sustained expression of insulin. In contrast to transgenic tadpole experiments, the conversion was partial and liver-specific gene expressions including those of albumin and transferrin were maintained in insulin-producing cells.

Materials and methods

Recombinant adenoviruses. Murine PDX1 cDNA was cloned from a MIN6 cDNA library by PCR. Using PCR, the *ClaI* site was added to murine PDX1 cDNA, which was digested with *ClaI* and subcloned into VP16-N (kind gift from Dr. H. Kanamori) as described [14]. Recombinant adenoviruses containing wt-PDX1 and PDX1-VP16 cDNA were prepared as reported previously [15–17]. LacZ adenovirus was used as a control [18].

Animals. Male C57BL/6N mice were purchased from Clea (Tokyo, Japan), housed in an air-conditioned environment, with a 12-h light-dark cycle, and fed a regular unrestricted diet. Diabetes was induced by intraperitoneal injection of 160–170 mg/kg STZ (Sigma St. Louis, MO) in citrate buffer at 5–6 weeks of age. Blood glucose was determined after a 10 h fast at 6 days after STZ injection; mice with fasting glucose levels of 300–600 mg/dl were used for the experiments. The mice were treated with 2×10^8 plaque-forming units of recombinant adenovirus by systemic injection into the tail vein and killed 40 days after adenovirus injection. Serum insulin concentrations were measured using a rat insulin ELISA Kit Ultra Sensitive (Morinaga, Tokyo, Japan).

Oral glucose tolerance tests. Oral glucose tolerance tests were performed 40 days after adenovirus infusion. Serum glucose levels were determined before, and 15, 30, 60, 90, and 120 min after, administration of oral glucose (1 g/kg body weight).

Immunoblotting. Liver samples were homogenized in buffer (100 mM Tris, pH 8.5, 250 mM NaCl, 1% BP-40, and 1 mM EDTA). Tissue homogenates were centrifuged at 14,000*g* for 10 min at 4 °C. Supernatants including tissue protein extracts (180 μg total protein) were then boiled in Laemmli buffer containing 10 mM dithiothreitol. Aliquots of proteins (15 μg) were subjected to SDS–PAGE. Immunoblot analyses were performed using ECL plus a Western Blotting Detection System Kit (Amersham Buckinghamshire, UK). Antibodies to PDX1 (A-17, Santa Cruz Biotechnology, Santa Cruz, CA) and HSV-1 VP16 (vA-19, Santa Cruz Biotechnology) were commercially obtained.

Immunohistochemistry. Livers of mice were excised 40 days after adenoviral treatment and fixed overnight in 10% paraformaldehyde. Fixed tissues were processed for paraffin embedding and 3 μm sections were prepared. For immunohistochemistry, the streptavidin–biotin (SAB) method was performed using a Histofine SAB-PO kit (Nichirei, Tokyo, Japan) for insulin, glucagon, and amylase, and a MAX-PO kit (Nichirei) for somatostatin, and an EnVision kit/HRP (DAKO, Glostrup, Denmark) for pancreatic polypeptide. Slides were deparaffinized, and then were either autoclaved in citrate buffer for antigen retrieval before being incubated in blocking solution (for amylase, somatostatin, and pancreatic polypeptide detection), or immediately exposed to the blocking solution (for insulin and glucagon detection). For insulin detection, sections were incubated for 18 h at 4 °C with monoclonal antibody against human insulin (Sigma) diluted 1:1000 in PBS. For detection of glucagon, sections were incubated for 18 h at 4 °C with antiserum raised against human glucagon (DAKO) diluted 1:3000 in PBS. For detection of somatostatin, sections were incubated overnight at 4 °C with rat anti-somatostatin monoclonal antibody (Chemicon, Temecula, CA) diluted 1:100 in PBS. For detection of pancreatic polypeptide, sections were incubated overnight at 4 °C with antiserum raised against rat pancreatic polypeptide (LINCO, St. Charles, MO) diluted 1:100 in PBS. For detection of amylase, sections were incubated for 18 h at 4 °C with antiserum raised against the C-terminus of human amylase (Santa Cruz Biotechnology) diluted 1:1000 in PBS. Slides were then incubated with the biotinylated IgG for 1 h and next with peroxidase-conjugated streptavidin for 30 min at room temperature. Finally, immunoreactivity was visualized by incubation with a substrate solution containing 3,3′-diaminobenzidine tetrahydrochloride (DAB).

Fluorescent immunocytochemistry. The 3 μm sections of paraffin-embedded liver were processed as follows. For double staining of